

---

*Research Article: New Research | Novel Tools and Methods*

## **SIGNAL PROPAGATION VIA OPEN-LOOP INTRATHALAMIC ARCHITECTURES: A COMPUTATIONAL MODEL**

<https://doi.org/10.1523/ENEURO.0441-19.2020>

**Cite as:** eNeuro 2020; 10.1523/ENEURO.0441-19.2020

Received: 25 October 2019

Revised: 13 January 2020

Accepted: 20 January 2020

---

*This Early Release article has been peer-reviewed and accepted, but has not been through the composition and copyediting processes. The final version may differ slightly in style or formatting and will contain links to any extended data.*

**Alerts:** Sign up at [www.eneuro.org/alerts](http://www.eneuro.org/alerts) to receive customized email alerts when the fully formatted version of this article is published.

Copyright © 2020 Brown et al.

This is an open-access article distributed under the terms of the Creative Commons Attribution 4.0 International license, which permits unrestricted use, distribution and reproduction in any medium provided that the original work is properly attributed.

1 SIGNAL PROPAGATION VIA OPEN-LOOP INTRATHALAMIC ARCHITECTURES:

2 A COMPUTATIONAL MODEL

3 Abbreviated Title: Signaling via open-loop thalamic architectures

4  
5 Jeffrey W. Brown<sup>1</sup>, Aynaz Taheri<sup>2</sup>, Robert V. Kenyon<sup>2</sup>, Tanya Berger-Wolf<sup>2</sup>, and Daniel A. Llano<sup>1,3,4,5,\*</sup>

6  
7 1. College of Medicine, University of Illinois at Urbana-Champaign, Urbana, IL 61801, USA

8 2. Department of Computer Science, University of Illinois at Chicago, Chicago, IL 60607, USA

9 3. Beckman Institute for Advanced Science and Technology, University of Illinois at Urbana-  
10 Champaign, Urbana, IL 61801, USA

11 4. Neuroscience Program, University of Illinois at Urbana-Champaign, Urbana, IL 61801, USA

12 5. Department of Molecular and Integrative Physiology, University of Illinois at Urbana-Champaign,  
13 Urbana, IL 61801, USA

14  
15 \*Corresponding Author:

16 Daniel A. Llano, M.D., Ph.D.

17 2355 Beckman Institute

18 405 North Mathews Avenue

19 Urbana, IL 61801

20 [d-llano@illinois.edu](mailto:d-llano@illinois.edu)

21  
22 Number of Figures: 4

23 Number of Tables: 4

24 Number of Words for Abstract: 223

25 Number of Words for Introduction: 629

26 Number of Words for Discussion: 2,402

27 Acknowledgments: We acknowledge funding through the National Science Foundation (1515587 to  
28 D.A.L., R.V.K., and T.B.-W.). We thank Profs. Thomas Anastasio, Ruoqing Zhu, and Rama Ratnam, Drs.  
29 Kush Paul and Baher Ibrahim, and Mr. Weddie Jackson for their valuable analytical, statistical, and  
30 technical insights. We also extend our gratitude to former Regional Dean M. Michele Mariscalco of the  
31 University of Illinois College of Medicine for enabling the collaboration between J.W.B. and D.A.L. This  
32 work made use of the Illinois Campus Cluster, a computing resource that is operated by the Illinois  
33 Campus Cluster Program (ICCP) in conjunction with the National Center for Supercomputing  
34 Applications (NCSA) and which is supported by funds from the University of Illinois at Urbana-  
35 Champaign. J.W.B.'s current affiliation is with the Center for Brain Function and Repair, Rosalind  
36 Franklin University of Medicine and Science, North Chicago, IL 60064, USA.

37

38 Conflict of Interest Statement: The authors declare no competing financial interests.

39

40 Funding Sources: National Science Foundation 1515587 (D.A.L., R.V.K., T.B.-W.)

41 **Abstract:**

42 Propagation of signals across the cerebral cortex is a core component of many cognitive processes and is  
43 generally thought to be mediated by direct intracortical connectivity. The thalamus, by contrast, is  
44 considered to be devoid of internal connections and organized as a collection of parallel inputs to the  
45 cortex. Here, we provide evidence that “open-loop” intrathalamic pathways involving the thalamic  
46 reticular nucleus (TRN) can support propagation of oscillatory activity across the cortex. Recent studies  
47 support the existence of open-loop thalamo-reticulo-thalamic (TC-TRN-TC) synaptic motifs in addition  
48 to traditional closed-loop architectures. We hypothesized that open-loop structural modules, when  
49 connected in series, might underlie thalamic and, therefore cortical, signal propagation. Using a  
50 supercomputing platform to simulate thousands of permutations of a thalamocortical network based on  
51 physiological data collected in mice, rats, ferrets, and cats and in which select synapses were allowed to  
52 vary both by class and individually, we evaluated the relative capacities of closed- and open-loop TC-  
53 TRN-TC synaptic configurations to support both propagation and oscillation. We observed that 1) signal  
54 propagation was best supported in networks possessing strong open-loop TC-TRN-TC connectivity; 2)  
55 intracellular synapses were neither primary substrates of propagation nor oscillation; and 3)  
56 heterogeneous synaptic networks supported more robust propagation of oscillation than their  
57 homogeneous counterparts. These findings suggest that open-loop, heterogeneous intrathalamic  
58 architectures might complement direct intracortical connectivity to facilitate cortical signal propagation.

59

60 **Significance Statement:**

61 Interactions between the dorsal thalamus and thalamic reticular nucleus (TRN) are speculated to  
62 contribute to phenomena such as arousal, attention, sleep, and seizures. Despite the importance of the  
63 TRN, the synaptic microarchitectures forming the basis for dorsal thalamus-TRN interactions are not fully  
64 understood. The computational neural model we present incorporates “open-loop” thalamo-reticular-  
65 thalamic (TC-TRN-TC) synaptic motifs, which have been experimentally observed. We elucidate how  
66 open-loop motifs possess the capacity to shape the propagative properties of signals intrinsic to the

67 thalamus and evaluate the wave dynamics they support relative to closed-loop TC-TRN-TC pathways and  
68 intracellular synaptic connections. Our model also generates predictions regarding how different spatial  
69 distributions of reticulothalamic and intracellular synapses affect these signaling properties.

70

71 **Introduction:**

72 Propagation of activity across the cerebral cortex is thought to underlie multiple cognitive processes, as  
73 well as pathological processes such as epilepsy and migraine (Leao, 1944; Muller et al., 2014, 2016;  
74 Kokkinos et al., 2017). Cortical regions are highly interconnected via direct axonal projections as well as  
75 via polysynaptic pathways involving the basal ganglia and thalamus (Parent and Hazrati, 1995; Theyel et  
76 al., 2010). Cortical signal propagation is generally thought to be mediated via direct cortical connections  
77 (Felleman and Van Essen, 1991; Kötter and Sommer, 2000), but recent evidence suggests that the  
78 thalamus serves as a control point to modify cortical activity during cognitive processes such as  
79 attentional shifting (Wimmer et al., 2015). An advantage of a thalamic mode of signal propagation is the  
80 efficiency by which modulatory influences may control thalamic, and therefore cortical, propagation. The  
81 thalamus, however, is generally thought to have limited internal connectivity and therefore limited  
82 capacity to serve as a substrate for signal propagation.

83

84 A major intermediary allowing for communication between thalamocortical neurons, the thalamic  
85 reticular nucleus (TRN), is a sheet of GABAergic neurons that partially envelops the dorsal thalamus  
86 (Pinault, 2004). It has been speculated to participate in phenomena ranging from selective attention  
87 (Crick, 1984; Guillery et al., 1998; McAlonan et al., 2006) to sleep and arousal (Linás and Paré, 1991,  
88 Steriade et al., 1993; Guillery et al., 1998; McAlonan et al., 2006) and fear responses (Dong et al., 2019),  
89 and may play a role in generating absence seizures (von Krosigk et al., 1993; Bal et al., 1995; Destexhe et  
90 al., 1996a; Huguenard, 1998; McCormick and Contreras, 2001), symptoms of neurodevelopmental  
91 disorders (Wells et al., 2016; Krol et al., 2018), and schizophrenia (Ferrarelli and Tononi, 2011). The

92 TRN projects exclusively to TC neurons, while receiving reciprocal, glutamatergic thalamoreticular (TC-  
93 TRN) connections (Sherman and Guillery, 2001).

94

95 The structural microarchitecture of bidirectional pathways connecting the dorsal thalamus and TRN has  
96 been the subject of ongoing debate. It was originally assumed that thalamo-reticulo-thalamic (TC-TRN-  
97 TC) pathways were reciprocal, forming “closed loops” of recurrent inhibition delivered to TC neurons  
98 (Figure 1A, left) (Hale et al., 1982; Steriade et al., 1993; Warren et al., 1994; Sherman and Guillery,  
99 1996; Pinault, 2004). While closed disynaptic loops have indeed been confirmed, they were only  
100 identified in a minority of examined TC-TRN pairs (Shosaku, 1986; Lo and Sherman, 1994; Pinault and  
101 Deschênes, 1998; FitzGibbon et al., 2000; Gentet and Ulrich, 2003; Pinault, 2004). Another connectional  
102 scheme between the dorsal thalamus and TRN is the so-called “open-loop” TC-TRN-TC pathway,  
103 wherein a TC neuron is not reciprocally inhibited by the TRN neuron it excites (Figure 1A, right). Open-  
104 loop configurations have been inferred from recordings in rodent thalamic slice preparations (Crabtree et  
105 al., 1998; Crabtree and Isaac, 2002; Lam and Sherman, 2005, 2015; Lee et al., 2010) and confirmed in  
106 anatomical studies (Pinault and Deschênes, 1998; Kimura et al., 2007; Kimura, 2014). Furthermore, open-  
107 loop pathway variants in the form of X-TRN-TC are also known to exist, with X representing indirect  
108 sources of modulation to the sensory thalamus via the TRN, including monoaminergic and cholinergic  
109 brainstem nuclei, GABAergic nuclei of the basal forebrain, the amygdala, and prefrontal cortex (Morrison  
110 and Foote, 1986; Hallanger et al., 1987; Asanuma and Porter, 1990; Bickford et al., 1994; Zikopoulos and  
111 Barbas, 2006; Sun et al., 2013; Pita-Almenar et al., 2014; Wimmer et al., 2015).

112

113 Based on previous studies of open-loop TC-TRN-TC synaptic organization, we hypothesized that open-  
114 loop synaptic modules might underlie intrathalamic and therefore intracortical signal propagation.

115 Accordingly, we systematically examined thousands of permutations of a novel network model

116 comprising thalamic, reticular, and thalamorecipient, layer-4 cortical (Co) neurons to evaluate the

117 efficacy of known thalamic synaptic motifs (open-loop pathways, closed-loop pathways, and chemical

118 and electrical intrareticular synapses), in isolation and in combination, in mediating signal transmission  
119 across the thalamus and cortex.

120

121 **Materials and Methods:**

122 *Network architecture and simulations*

123 We constructed a baseline model network based on Willis et al. (2015) by connecting in series three  
124 thalamocortical pathways, each consisting of a TC, TRN, and layer-4 Co neuron (for a 3-by-3 neuron  
125 network); the physiological data utilized in our model were collected in mice, rats, ferrets, and cats of  
126 both sexes. Permutations of the baseline network potentially featured both closed- and/or open-loop TC-  
127 TRN-TC motifs, with the latter constituting one mode of connectivity between parallel thalamocortical  
128 pathways. Intrareticular synapses represented the other connections between pathways, based on the  
129 identification of both GABAergic (Ahlsén and Lindström, 1982; Steriade et al., 1990; Cox et al., 1996;  
130 Sanchez-Vives et al., 1997; Shu and McCormick, 2002; Deleuze and Huguenard, 2006; Lam et al., 2006)  
131 and electrical synapses (Landisman et al., 2002; Fuentealba et al., 2004; Long et al., 2004; Deleuze and  
132 Huguenard, 2006; Lam et al., 2006) between TRN neurons. Thus, we included three different  
133 polysynaptic configurations between thalamocortical pathways in our network (Figure 1B, from left to  
134 right): 1) those with a GABAergic intrareticular synapse (TRN-TRN<sub>GABA</sub>); 2) those with an electrical  
135 intrareticular synapse (TRN-TRN<sub>Elec</sub>); and 3) open-loop TC-TRN-TC pathways. Thalamic, reticular, and  
136 cortical cell layers were aligned topographically, such that TC<sub>1</sub> projected to both TRN<sub>1</sub> and Co<sub>1</sub> (Jones,  
137 1975; Steriade et al., 1993; Destexhe et al., 1998; Sohal et al., 2000; Sherman and Guillery, 2001). The  
138 divergence of thalamic and reticular synapses in the model was constrained to accommodate open-loop  
139 TC-TRN-TC architectures, which depend on a lack of recurrent feedback to the downstream TC neuron,  
140 in a subset of the simulated network variants: to this end, every TC neuron projected to exactly one TRN  
141 neuron, while single TRN neurons could project to either one TC neuron (whether recurrently or  
142 laterally), as in the case of entirely closed- or open-looped TC-TRN-TC motifs, or two TC neurons (one

143 recurrently and one laterally), if participating in a pathway expressing some intermediate degree of  
144 openness (Figure 1C).

145

146 To analyze how each variety of inter-pathway connection contributed to network dynamics, permutations  
147 of the baseline network were generated by varying three synaptic properties associated with each of the  
148 inter-pathway synaptic motifs; moreover, these parameters were either varied in a homogeneous or  
149 heterogeneous manner. In the case of homogeneously varied synaptic network permutations, the synaptic  
150 parameters associated with three inter-pathway motifs varied uniformly as a class, with all external, TC-  
151 TRN, and thalamocortical (TC-Co) synaptic conductances held constant: 1) TRN-TRN<sub>GABA</sub> synapses  
152 ranged in conductance between 0 and 450 nS; 2) TRN-TRN<sub>Elec</sub> synapses ranged in coupling coefficient  
153 between 0 and 0.36; and 3) a TC-TRN-TC “openness” coefficient, defined as the weight distribution of  
154 lateral vs. recurrent reticulothalamic (TRN-TC) connectivity, varied between 0 (completely closed-loop)  
155 and 1.0 (completely open-loop) and with a baseline TRN-TC conductance of 80 nS. Thus, for a network  
156 variant possessing an openness coefficient of 0.4 (i.e., exhibiting slightly more closed- than open-loop  
157 TC-TRN-TC connectivity), the laterally inhibitory TRN-TC synapses in the network, TRN<sub>1</sub>→TC<sub>2</sub> and  
158 TRN<sub>2</sub>→TC<sub>3</sub>, would carry a conductance of 32 nS (0.4\*80 nS), while the recurrent TRN-TC synapses,  
159 TRN<sub>1</sub>→TC<sub>1</sub>, TRN<sub>2</sub>→TC<sub>2</sub>, and TRN<sub>3</sub>→TC<sub>3</sub>, would exhibit a conductance of 48 nS (0.6\*80 nS). For the  
160 heterogeneously varied synaptic network variants, all TRN-TRN and TRN-TC synapses were allowed to  
161 vary independently. Domains for each of the synaptic variables were selected to include the range of  
162 conductance or coupling strengths reported in physiological measurements and/or used in similar neural  
163 models (Destexhe et al., 1996a, 1998; Sohal and Huguenard, 1998; Sohal et al., 2000; Landisman et al.,  
164 2002; Long et al., 2004; Traub et al., 2005).

165

166 Ongoing afferent synaptic input was delivered to every TC neuron in the model as Poisson-modulated  
167 spike trains centered at 40 Hz. An additional 200-Hz pulse train was applied to neuron TC<sub>1</sub> between  
168  $t=0.400$  and  $t=1.500$  s during every network simulation run. This high-frequency stimulus was modeled

169 on those used to elicit spindle-like waves in a ferret thalamoreticular slice preparation (Bal et al., 1995;  
 170 Kim et al., 1995). A given network’s output was compiled by assembling spike histograms (10-ms bins)  
 171 averaging 1,000 simulations for every cortical neuron (Figure 1D). We quantified network dynamics as a  
 172 function of variable TC-TRN-TC and intrareticular synaptic architectures by defining and measuring two  
 173 properties inherent to stimulus-evoked responses in each network variant: propagation and oscillation,  
 174 with the latter included in light of the fact that many characterized thalamic waveforms both oscillate and  
 175 propagate through the thalamus and cortex (Sherman and Guillery, 2001). Network properties were  
 176 quantified in the most downstream element of the cortical output layer, Co<sub>3</sub>. Propagation across a network  
 177 was quantified as the amplitude of the initial stimulus-evoked response in the detrended Co<sub>3</sub> histogram.  
 178 The degree of oscillation supported by each network permutation was defined as the amplitude of the first  
 179 off-center peak in the normalized autocorrelogram of post-stimulation activity (Figure 1D). Both  
 180 propagation and oscillation scores are reported as normalized to the maximum scores tabulated for each  
 181 property. Given the high prevalence of propagating oscillatory waves in the cerebral cortex (reviewed in  
 182 Muller et al., 2018), we furthermore defined a composite “optimization” (*Op*) metric to measure the  
 183 capacity of networks to simultaneously support and balance between propagation (*Pr*) and oscillation  
 184 (*Os*):

$$185 \quad Op = \sqrt{Pr^2 + Os^2} - |Pr - Os| \quad (1)$$

186

### 187 *Intrinsic neuronal models*

188 Single-compartment TC, TRN, and cortical model neurons obeyed Hodgkin-Huxley kinetics, with  
 189 membrane potentials  $V$  varying according to the first-order differential equation

$$190 \quad C \frac{dV}{dt} = -g_L(V - E_L) - \sum_i g_i(V)(V - E_i) \quad (2)$$

191 where  $C$  is the membrane capacitance,  $g_L$  and  $E_L$  are the leakage conductance and reversal potential,  
 192 respectively, and  $g_i(V)$  and  $E_i$  are the dynamic conductance and reversal potential, respectively, of the  $i$ th  
 193 voltage-gated, ligand-gated (chemical synaptic), or electrical synaptic conductance (for electrical synaptic

194 conductances, the effective reversal potential is equal to the presynaptic membrane potential; see  
195 Equation 3a). All three varieties of model neurons expressed both the standard transient sodium ( $I_{Na}$ ) and  
196 delayed-rectifier potassium ( $I_K$ ) currents. TC and TRN neurons additionally included a T-type calcium  
197 conductance (T-current;  $I_T$ ) and hyperpolarization-activated cation current (H-current;  $I_H$ ), following the  
198 TC model of Deleuze et al. (2012). Both TRN and layer-4 Co cells expressed a slow, non-inactivating  
199 potassium conductance ( $I_M$ ), following the modeling of Popischil et al. (2008), which accounts for the  
200 spike-frequency adaptation previously reported in physiological recordings from these neurons (Yamada  
201 et al., 1989; Willis et al., 2015). A list of intrinsic model cell parameters, including current conductances,  
202 reversal potentials, selected gating kinetics, and membrane capacitance, can be found in Table 1.

203

#### 204 *Synaptic models*

205 The kinetics of chemical synapses in our model network conformed to the synaptic depression model of  
206 Tdosdyks and Markram (1997). This model presupposes a finite quantity of “resources,” akin to synaptic  
207 vesicles, capable of being released by the presynaptic neuron; these resources can exist in an active,  
208 inactive, or recovered state. A parameter  $U_{SE}$  characterizes the fraction of recovered resources that can be  
209 converted to an active state (i.e., for release by the presynaptic neuron) following action potential  
210 induction in the presynaptic axon terminal(s). Following resource activation, synapses inactivate  
211 according to the time constant  $\tau_{inact}$ ; resources become available again for activation after a recovery  
212 period described by the time constant  $\tau_{recov}$ . These parameters, along with the neurotransmitters,  
213 postsynaptic conductances, and reversal potentials characterizing all of the chemical synapses in our  
214 model, are given in Table 2.

215

216 Glutamatergic TC-TRN and TC-Co and baseline GABAergic TRN-TC synaptic parameters matched  
217 those of Willis et al. (2015), with the latter synapses allowed to vary in conductance as described above.  
218 TRN-TC signaling was mediated exclusively through GABA<sub>A</sub> receptors, mirroring other thalamic and  
219 thalamocortical models in which the slower TRN-TC GABA<sub>B</sub> conductance was omitted (Traub et al.,

220 2005; Rogala et al., 2013; Pham and Haas, 2018). Although evidence has been presented challenging the  
 221 existence of GABAergic intrareticular synapses in certain mammalian species and age groups (Pinault et  
 222 al., 1997; Landisman et al., 2002; Pinault, 2004; Cruikshank et al., 2010; Hou et al., 2016), our model  
 223 avoided making assumptions regarding their presence, strength, or spatial distribution by allowing the  
 224 associated synaptic conductances to vary over a range of physiological values, including zero, and in  
 225 distribution. The reversal potential, conductance, and kinetics of the external synapses projecting to the  
 226 TC neurons were directly based on retinogeniculate synapses (Chen and Regehr, 2003), although the  
 227 generic nature of the external inputs in our model allows them to represent not only immediately upstream  
 228 sensory input but also brainstem modulation (e.g., serotonergic, adrenergic) known to act on thalamic  
 229 nuclei (Siegel and Sapru, 2015).

230

231 Electrical synapses between TRN neurons were based on the Cx36-dependent intrareticular gap junctions  
 232 first identified by Landisman et al. (2002). For TRN neurons, the sum of electrical synaptic currents ( $I_{Elec}$ )  
 233 entering any postsynaptic neuron  $j$  from presynaptic neuron(s)  $i$  was included in the rightmost term from  
 234 Equation 2 and calculated as

$$235 \quad I_{Elec(j)} = \sum_i g_{ij} (V_j - V_i) \quad (3a)$$

236 where  $g_{ij}$ , the gap junction conductance, was itself calculated as

$$237 \quad g_{ij} = D(x) \frac{g_j}{1/CC - 1} \quad (3b)$$

238 where  $CC$  was the electrical coupling coefficient between TRN neurons  $i$  and  $j$ ,  $g_j$  was the membrane  
 239 conductance of the postsynaptic neuron, and  $D(x)$  was a scaling factor that depended on the physical  
 240 distance between the coupled TRN neurons (Dayan and Abbott, 2005; Shimizu and Stopfer, 2013).

241 Although the individual gap junctions comprising TRN-TRN<sub>Elec</sub> synapses used in the model were not  
 242 explicitly coded for, differences in TRN-TRN coupling between different electrical synapses and network  
 243 permutations implicitly reflected differing gap junction densities, following Traub et al. (2005). TRN-  
 244 TRN<sub>Elec</sub> synapses were symmetrical (non-rectifying), such that  $g_{ij} = g_{ji}$ .

245

246 We extrapolated the attenuation of intracellular synaptic strength as a function of intracellular distance  
247 based on mappings of intrinsic connections within the TRN along a horizontal (anteroposterior) plane  
248 assembled by Deleuze and Huguenard (2006). Assuming 1) an intracellular distance of 50  $\mu\text{m}$  between  
249 adjacent TRN neurons, 2) a distance  $x$  (in multiples of 50  $\mu\text{m}$ ) between non-adjacent neurons, and 3) a  
250 Gaussian falloff in synaptic strength (Sohal et al., 2000), the baseline (adjacent-neuron) conductances of  
251 TRN-TRN<sub>GABA</sub> and TRN-TRN<sub>Elec</sub> synapses were scaled for non-adjacent synapses using the function

$$252 \quad D(x) = e^{-\frac{x^2}{2\lambda^2}} \quad (4)$$

253 where  $\lambda_{\text{GABA}}=531 \mu\text{m}$  and  $\lambda_{\text{Elec}}=130 \mu\text{m}$ .

254

255 Given the small spatial scale of our model, synaptic delays associated with finite axonal conductance  
256 times within the TRN and between the TRN and dorsal thalamus were disregarded, mirroring the  
257 simplification incorporated into previous thalamic and thalamocortical models simulating synaptic  
258 interactions on the order of 100 microns (Golomb et al., 1996; Traub et al., 2005). Although small (~1  
259 ms) thalamocortical delays were inserted into the network model of Traub et al. (2005), these were  
260 likewise omitted on the basis of the cortex functioning solely as an output layer in our model.

261

### 262 *Quantification and statistical analysis*

263 Our model was coded, simulated, and analyzed in MATLAB R2018b (MathWorks, Natick, MA),  
264 utilizing both a Dell Inspiron 3847 and Hewlett-Packard Z840 running Windows 10 and nodes on the  
265 Illinois Campus Cluster (National Center for Supercomputing Applications, University of Illinois at  
266 Urbana-Champaign). Simulations, of which there were 1,000 for every network permutation, employed  
267 0.1-ms time steps, with temporal integration based on the hybrid analytic-numeral integration method of  
268 Moore and Ramon (1974), which optimizes between accurate solutions to Hodgkin-Huxley and synaptic  
269 models and computational efficiency. All simulations commenced with a 200-ms equilibration period,

270 during which no external stimulation was delivered to TC neurons; this allowed all network elements to  
271 attain steady-state conditions. The number of homogeneously and heterogeneously varied synaptic  
272 network variants generated were 770 and 12,681, respectively.

273

274 Statistical analysis was performed in both MATLAB and R (R Core Team, 2013), with the *glmnet*  
275 package (Friedman et al., 2010) utilized within the latter platform to perform regression analyses.  
276 Multiple linear regression was employed to establish rudimentary relationships between synaptic classes  
277 (homogeneously synaptic networks) or individual synapses (heterogeneously synaptic networks) and each  
278 of the two studied network properties, even in instances where these relationships deviated from linearity.  
279 Second-order polynomial ( $2^{\circ}$ ) regression models with interaction terms elucidated how synaptic  
280 interactions and nonlinearities affected these network properties. Regressions were optimized using  
281 elastic net regularization, with the specific regularization hyperparameter  $\alpha$  selected to minimize each  
282 regression model's root-mean-square error. To convey the relative influence of different synaptic classes  
283 or individual synapses on dynamic network properties, all regression coefficients are reported here as  
284 normalized to the coefficient with the largest absolute value; the effects corresponding to NRCs with  
285 absolute values of less than 0.05 were disregarded as negligibly influential on network dynamics. Both  
286 unpaired Student *t*-tests and one-way analysis of variance (ANOVA) models were used to compare the  
287 mean property scores between different sets of networks, with Tukey's honestly significant difference  
288 tests used to ascertain pairwise difference between groups in the latter; standard errors of the mean were  
289 used a measure of variance, and null hypotheses were rejected at probability values (*p* values) below 0.05.  
290 Kolmogorov-Smirnov and Levene's tests were employed to confirm normality and homogeneity of  
291 variance, respectively, when utilizing parametric mean-comparison tests; data were transformed as  
292 needed to conform to these prerequisites.

293

294 *Code accessibility*

295 The code/software described in the paper is freely available online at  
296 <https://github.com/JeffreyWBrown/Open-loop-TC-TRN-TC>. The code is available as Extended Data.

297

298 **Results:**

299 *Propagation and oscillation in homogeneously varied synaptic models*

300 Stimulus-evoked responses propagated linearly across the length of homogeneous synaptic networks,  
301 occurring at average fixed intervals of  $93.31 \pm 0.35$  ms (mean  $\pm$  standard error of the mean; range, 60-110  
302 ms) between adjacent thalamocortical pathways, across all model permutations and with a mean velocity  
303 of 0.54 mm/s, assuming a 50  $\mu$ m separation between adjacent neurons in each network layer. All 770  
304 homogeneous network variants were ranked according to their cortical propagation scores (Figure 2A,  
305 top). TC neurons exhibited both tonic firing and bursting activity, with the former mode more frequently  
306 observed (Figure 2B).

307

308 Multiple linear regression analysis ( $R^2=0.793$ , root-mean-square-error or RMSE=0.047,  $p<0.0001$ )  
309 demonstrated a strong positive correlation between the TC-TRN-TC openness coefficient and propagation  
310 score (normalized regression coefficient or NRC=1.000). By contrast, chemical and electrical TRN-TRN  
311 synaptic connectivity tended to modestly diminish propagation (NRC=-0.173 and NRC=-0.136,  
312 respectively; see Table 3). Further, other excitatory connectivity, such as cortico-cortical or  
313 corticothalamic connectivity, often postulated as being important for cortical signal propagation  
314 (Felleman and Van Essen, 1991; Kötter and Sommer, 2000; Theyel et al., 2010), was not necessary. Thus,  
315 the homogeneously varied synaptic network permutations that best accommodated signal propagation  
316 were generally ones with weak or absent synapses between TRN neurons and strong open-loop TC-TRN-  
317 TC connections. For example, Network  $\alpha$ , which epitomizes this architecture, exhibited robust signal  
318 propagation in response to a fixed stimulus delivered to TC<sub>1</sub>; a representative simulation of this network  
319 is shown in Figure 2B, left, and its position within the parameter space depicted in left-sided heat map of

320 Figure 2C is labeled. Stimulus-evoked activity in this network tended to propagate efficiently from Co<sub>1</sub> to  
321 Co<sub>3</sub>; near-synchronous propagation cascades were elicited in both the TRN and cortical layers of the  
322 model, having been stimulated by propagating activity in upstream TC neurons. Smooth, linear  
323 propagation of action potentials across the network depended on the synchronous induction of inhibitory  
324 postsynaptic potentials (IPSPs) and the ensuing post-inhibitory rebound spikes in TC neurons, as  
325 mediated by T-type Ca<sup>2+</sup> channels and driven by inhibition from the TRN, which occurred reliably and at  
326 fixed intervals in Network  $\alpha$ . Relative to Network  $\alpha$ , other network permutations exhibiting stronger  
327 intracellular synapses did not support propagation as efficiently. We surmise that TRN-TRN<sub>GABA</sub>  
328 synaptic connections reduced the incidence of IPSPs in TC neurons required for signal propagation across  
329 the network, while electrical coupling between TRN neurons destructively shunted a propagating signal  
330 away from the thalamoreticular lattice through which it predominantly traversed the network.

331

332 A 2<sup>o</sup> regression model of propagation as a function of all three synaptic class variables ( $R^2=0.842$ ,  
333 RMSE=0.041,  $p<0.0001$ ; Table 3) revealed modestly negative interaction term between TRN-TRN<sub>Elec</sub>  
334 synapses and TC-TRN-TC openness (NRC=-0.365), indicating that in networks where both electrical  
335 synapses were strong and TC-TRN-TC openness high, the extent of supported propagation diminished  
336 nonlinearly; a smaller negative interaction between TRN-TRN<sub>GABA</sub> synapses and TC-TRN-TC openness  
337 was also observed (NRC=-0.152). Together, these terms suggested that propagation was more  
338 significantly affected by connections in the TRN layer within the more open-loop networks. This  
339 relationship was evident, for example, in the right-sided heat map of Figure 2C, in which propagation  
340 scores more markedly decreased with increasing TRN-TRN electrical coupling as TC-TRN-TC openness  
341 itself increased.

342

343 Oscillatory responses recurred in Co<sub>3</sub> neurons at a mean frequency of  $9.07 \pm 0.2$  Hz (range, 7.14-12.50  
344 Hz) across all homogeneous model permutations. Propagation and oscillation scores across all 770

345 homogeneous networks were strongly anticorrelated (Pearson's  $r=-0.671$ ,  $p<0.0001$ ). Accordingly,  
346 oscillation was best accommodated in network permutations exhibiting strongly closed-loop connectivity  
347 (Figure 2A, bottom); however, the capacity to support oscillation was neither markedly linear nor  
348 monotonically decreasing as a function of increasing openness coefficient (Figure 2D). Rather, a one-way  
349 ANOVA with Tukey's tests revealed that, on average, oscillation scores peaked and remained statistically  
350 indistinguishable from one another across the subset of network permutations with openness coefficients  
351 between 0 and 0.4, with scores then decreasing in a roughly linear fashion with increasing TC-TRN-TC  
352 openness [ $F(10,759)=137.8$ ,  $p<0.0001$ ]; this result was consistent with a 2° regression model of  
353 oscillation ( $R^2=0.630$ ,  $RMSE=0.128$ ,  $p<0.0001$ ; Table 3), in which the linear and quadratic terms in TC-  
354 TRN-TC openness were associated with NRCs of -1.000 and -0.052, respectively, and the effects of  
355 TRN-TRN<sub>GABA</sub> (NRC=0.060) and TRN-TRN<sub>Elec</sub> (NRC regularized to 0) on oscillation were weakly  
356 positive and negligible, respectively. Taken with the analysis of propagation, these data suggest that  
357 networks with mixed open- and closed-loop connectivity (which is likely close to physiological reality)  
358 can support the coexistence of oscillation and propagation (see *Propagation and oscillation in*  
359 *heterogeneously varied synaptic models*, below).

360

361 The predominant mechanism by which oscillation arose in Co<sub>3</sub> was through post-inhibitory rebound in  
362 TC<sub>3</sub>, as engendered by the strong recurrent inhibition found in network permutations exhibiting primarily  
363 closed-loop TC-TRN-TC connectivity. This mode of oscillation was exemplified by Network β, a  
364 strongly closed-loop network variant. In the simulation shown of this network (Figure 2B, right),  
365 oscillatory activity was enabled by a single epoch of signal propagation. Notably, neither the presence of  
366 strong GABAergic nor electrical intracellular synapses in Network β exerted much effect on its ability to  
367 support oscillation, as predicted by the 2° regression model.

368

369 *Propagation and oscillation in heterogeneously varied synaptic models*

370 Recent studies have highlighted heterogeneity in TRN neuronal connectivity, synaptic physiology and  
371 chemical identities (Lee et al., 2007; Halassa et al., 2014; Clemente-Perez et al., 2017). We therefore  
372 examined the impact of allowing all synaptic connections involving the TRN to be independently varied.  
373 We constructed circuit-level schematics of linear regression models for propagation (Figure 3A, top) and  
374 oscillation (Figure 3A, bottom) as functions of the 14 synaptic variables in heterogeneous networks.  
375  
376 Propagation in heterogeneously varied synaptic networks increased chiefly as a function of increasing the  
377 strength of the more downstream of the two laterally inhibitory TRN-TC synapses,  $TRN_2 \rightarrow TC_3$ : the  
378 corresponding term in a linear regression model of propagation ( $R^2=0.742$ ,  $RMSE=0.069$ ,  $p<0.0001$ ; see  
379 Table 4) possessed an NRC of 1.000 (Figure 3A, top). Propagation scores also scaled to a lesser extent  
380 with the more upstream laterally inhibitory reticulothalamic synapse,  $TRN_1 \rightarrow TC_2$  (NRC=0.608). The two  
381 inhibitory intrareticular synapses originating at the rightmost end of the model network,  $TRN_3 \rightarrow TRN_1$   
382 and  $TRN_3 \rightarrow TRN_2$ , both exerted a small negative effect on propagation (NRC=-0.087 and NRC=-0.084,  
383 respectively). Additionally, two TRN- $TRN_{Elec}$  synapses,  $TRN_1=TRN_2$  and  $TRN_1=TRN_3$  (where the “=”  
384 denotes an electrical synapses), marginally decremented propagation in heterogeneous networks, with  
385 NRCs of -0.051 and -0.072, respectively. These findings at an individual synaptic level comported with  
386 the observation that strong TRN-TRN interactions, whether chemical or electrical, tended to impede  
387 signal propagation in homogeneous network variants.  
388  
389 A 2<sup>o</sup> regression model ( $R^2=0.857$ ,  $RMSE=0.051$ ,  $p<0.0001$ ; Table 4) disclosed a large, propagation-  
390 enhancing interaction between the two laterally inhibitory synapses (NRC=0.753), underscoring the same  
391 dependence of propagation on strong open-loop TC-TRN-TC connectivity as seen in homogeneously  
392 synaptic networks, but additionally demonstrating that propagation scores increased nonlinearly as a  
393 function of simultaneously increasing the weights of  $TRN_1 \rightarrow TC_2$  and  $TRN_2 \rightarrow TC_3$ . Interactions between  
394 TRN-TRN synapses of either variety and TRN-TC synapses tended diminish propagation, as did those  
395 between recurrent and lateral inhibitory TRN-TC synapses. Taken together, the linear and 2<sup>o</sup> regression

396 models indicated that heterogeneous network permutations with strong laterally inhibitory TRN-TC  
397 synapses tended to best support propagation. Consistent response propagation across the length of the  
398 network was epitomized by Network  $\alpha'$ , in which  $\text{TRN}_1 \rightarrow \text{TC}_2$  and  $\text{TRN}_2 \rightarrow \text{TC}_3$  were both relatively  
399 strong and those synapses impeding propagation comparatively weak (Figure 3B, left).

400

401 *Heterogeneously varied synaptic architectures better supported propagation of oscillation*

402 In contrast to the homogeneous models, there was a very small negative correlation between the  
403 propagation and oscillation scores of these networks ( $r=-0.0296$ ,  $p=0.0008$ ), suggesting that propagation  
404 and oscillation more easily coexist in heterogeneous than homogeneous models. This supposition was  
405 confirmed through a 2° regression analysis ( $R^2=0.388$ ,  $\text{RMSE}=0.118$ ,  $p<0.0001$ ), which suggested that  
406 interactions between recurrently and laterally inhibitory TRN-TC synapses (NRCs ranging between 0.345  
407 and 0.669) facilitated the propagation of oscillation, a mechanism typified by Network  $\beta'$  (Figure 3B,  
408 right). Two intrareticular synapses,  $\text{TRN}_1\text{-TRN}_3$  and  $\text{TRN}_1=\text{TRN}_3$ , tended to contribute modestly to  
409 oscillation (NRCs of 0.115 and 0.117, respectively, in the linear regression model,  $R^2=0.253$ ,  
410  $\text{RMSE}=0.131$ ,  $p<0.0001$ ; Figure 3A, bottom), while, in their individual capacities,  $\text{TRN}_1 \rightarrow \text{TC}_2$  and  
411  $\text{TRN}_2 \rightarrow \text{TC}_3$  diminished oscillation (NRCs of -1.000 and -0.892, respectively).

412

413 We analyzed the relative capacities of homogeneously and heterogeneously varied synaptic networks to  
414 support propagation, oscillation, and optimization by comparing the 20 highest scores achieved by  
415 homogeneous and heterogeneous network permutations with respect to each performance metric. No  
416 significant differences in mean propagation scores between top-performing homogeneous and  
417 heterogeneous networks were disclosed [unpaired  $t$ -test,  $t(38)=0.46$ ,  $p=0.647$ ; Figure 4]. We attributed  
418 this lack of differences to the fact that network permutations in which the synapses  $\text{TRN}_1 \rightarrow \text{TC}_2$  and  
419  $\text{TRN}_2 \rightarrow \text{TC}_3$  were both maximally weighted would be equally capable of supporting robust signal  
420 propagation, regardless of whether these synapses were varied homogeneously or heterogeneously. By

421 contrast, top-scoring heterogeneous network variants better supported both oscillation [ $t(38)=13.88$ ,  
422  $p<0.0001$ ] and optimization [ $t(38)=18.04$ ,  $p<0.0001$ ] than their homogeneous counterparts. Because  
423 networks supporting the propagation of oscillatory activity would, by definition, score high with respect  
424 to optimization, these results not only confirmed that heterogeneous networks were more likely than  
425 homogeneous networks to accommodate this oscillatory mechanism, but furthermore disclosed that  
426 propagation of oscillation across the thalamocortical network was associated with higher oscillation  
427 scores than post-inhibitory-driven oscillation in TC<sub>3</sub>, the predominant form of oscillation observed in  
428 homogeneous networks.

429

430 **Discussion:**

431 The presented analysis suggests that open-loop TC-TRN-TC synaptic motifs (Figure 1B, right) could  
432 function as a substrate for signal propagation across the thalamus, and by extension, cortical networks  
433 without the need for direct cortico-cortical, intrareticular or corticothalamic connectivity. Post-inhibitory  
434 rebound mediated by T-type Ca<sup>2+</sup> channels served as a substrate for both propagation and oscillation in  
435 the simulated networks. TRN-TRN connections, either chemical or electrical (Figure 1B, left and middle),  
436 diminished horizontal propagation by disrupting the precise timing relationships required to propagate a  
437 signal across the network. Models with heterogeneously varied TRN synapses outperformed those whose  
438 synapses varied as a class with respect to the propagation of oscillatory activity, consistent with the  
439 emerging literature documenting cellular and synaptic heterogeneity in the TRN (Lee et al., 2007; Halassa  
440 et al., 2014; Clemente-Perez et al., 2017). These data suggest that widespread propagating thalamic or  
441 thalamocortical activity, under both pathological and physiological conditions, may be mediated, at least  
442 in part, by TC-TRN-TC connections. The model makes strong predictions that can be tested  
443 physiologically.

444

445 Like most of the thalamic (Destexhe et al., 1993, 1996a; Golomb et al., 1996; Bazhenov et al., 1998;  
446 Sohal and Huguenard, 1998) and thalamocortical models (Destexhe et al., 1998; Bazhenov et al., 2002;

447 Rogala et al., 2013) that inspired our model, we utilized single-compartment, Hodgkin-Huxley neurons.  
448 While these model cells contribute to the computational parsimony and practicality of network models,  
449 particularly where the analysis of network dynamics is prioritized, they neglect the intrinsic cable  
450 properties of real neurons and, relatedly, the spatially disparate nature of synaptic integration and  
451 heterogeneous expression of intrinsic and synaptic conductances (Dayan and Abbott, 2005; Herz et al.,  
452 2006). Such considerations are particularly relevant here relative to dendritic distributions of T- and H-  
453 currents in TC neurons (McCormick and Pape, 1980; Destexhe et al., 1998; Williams and Stuart, 2000;  
454 Traub et al., 2005) and TRN neurons (Contreras et al., 1993; Destexhe et al., 1996b; Traub et al., 2005;  
455 Crandall et al., 2010). Although multicompartment neuronal models incorporating such details could  
456 conceivably alter the network dynamics being studied, they were not necessary to simulate the  
457 propagation of oscillatory waves seen physiologically (Bal et al., 1995; Destexhe et al., 1996a; Golomb et  
458 al., 1996; Bazhenov et al., 1998; Sohal and Huguenard, 1998).

459

460 Additionally, the present model omitted explicit corticothalamic and corticoreticular synapses, both of  
461 which have been identified and physiologically characterized to varying degrees (Steriade et al., 1972;  
462 White and Hersch, 1982; De Curtis et al., 1989; Contreras et al., 1996; Blumenfeld and McCormick,  
463 2000; Zhang and Jones, 2004; Crandall et al., 2015), though the former were effectively amalgamated  
464 with both feedforward sensory and modulatory projections to the thalamus in the form of the Poisson-  
465 modulated external input we delivered to individual TC neurons. Both forms of feedback have been  
466 implicated in the spread of spindle waves and in the maintenance of their synchronization over large  
467 distance scales (on the order of the length of the mammalian forebrain) and are furthermore known to  
468 drive spindle wave formation and propagation in vivo by polysynaptically recruiting TC neurons via  
469 TRN-mediated post-inhibitory rebound (Steriade et al., 1972; Roy et al., 1984; Contreras et al., 1996;  
470 Contreras and Steriade, 1996; Suga and Ma, 2003; Sillito et al., 2006; Crandall et al., 2015; Sorokin et al.,  
471 2017). It should be noted, however, that short-range propagation of spindle waves, which can be elicited  
472 in isolated thalamic slice preparations (Bal et al., 1995; Kim et al., 1995), is preserved following

473 decortication, both in vivo and in silico (Contreras et al., 1996; Contreras and Steriade, 1996; Destexhe et  
474 al., 1998).

475

476 The signaling dynamics observed in our small-scale, broadly feedforward model would undoubtedly be  
477 altered by introducing corticothalamic and corticoreticular feedback, as well as cortico-cortical synapses:  
478 in particular, we can predict, based on other modeling studies that have systematically explored the  
479 contributions of such connections within fundamentally closed-loop thalamoreticular frameworks  
480 (Destexhe et al., 1998; Rogala et al., 2013), that cortical feedback to the dorsal thalamus and TRN would  
481 increase the frequency of post-inhibitory rebound in relay cells of the former, while also increasing  
482 oscillatory activity through the introduction of new recurrent pathways between the thalamus and cortex.  
483 While the enhancement of post-inhibitory rebound in the thalamus would a priori suggest an enhancement  
484 in the extent of signal propagation mediated through open TC-TRN-TC loops, our results demonstrate  
485 that the efficiency of such propagation can be attenuated by decohering activity introduced via  
486 intrareticular synapses: as such, whether corticothalamic, corticoreticular, and cortico-cortical synapses  
487 dynamics would ultimately enhance open-loop-mediated propagation or decrement it by interfering with  
488 the temporal dynamics underlying this form of intrathalamic signaling would heavily depend on, among  
489 other things, the degree to which these additional synapses spatially diverged within the dorsal thalamus  
490 and TRN. Notwithstanding elaborations of cortical projections within our network model, our present  
491 results suggest that open-loop TC-TRN-TC architectures may mediate a novel form of intrinsic thalamic,  
492 and by extension, cortical signal propagation that exists independently of top-down modulation (for  
493 example, in localized regions of the thalamus where cortical innervation is sparse) and potentially in  
494 parallel to the modes of thalamocortical propagation in which both corticofugal pathways and cortico-  
495 cortical synapses are known to participate. Future efforts within our modeling paradigm stand to  
496 incorporate reciprocal cortical projections involving one or multiple cortical layers (see, for example,  
497 Destexhe et al. 1998; Bahzenov et al., 2002; Traub et al., 2005; Izhikevich and Edelman, 2008; Rogala et  
498 al., 2013).

499

500 *Comparison to related computational models and physiological data*

501 Although the production of spindle waves was not an explicit objective of our study, some of the wave  
502 dynamics arising in our networks were nevertheless consistent with those inherent to spindle or spindle-  
503 like waves. Despite possessing higher degrees of TC→TRN and TRN→TC synaptic divergence and  
504 lacking the exclusively open-loop TC-TRN-TC architecture characterizing a subset of our network  
505 variants, other isolated thalamic models allowing for longitudinal wave propagation similarly  
506 accommodated this propagation along the lattice of interconnected TC and TRN neurons by way of  
507 laterally inhibitory TRN-TC synapses (Destexhe et al., 1996a; Golomb et al., 1996; Bazhenov et al.,  
508 1998); at short ranges, this mechanism of signal propagation also prevailed in larger-scale thalamocortical  
509 models, while corticothalamic projections acted to propagate activity to more distal sites (Destexhe et al.,  
510 1998; Destexhe and Sejnowski, 2003). Comparably, recurrently inhibitory TRN-TC synapses have been  
511 documented to play a vital role in the generation of oscillatory behavior in the thalamus (von Krosigk et  
512 al., 1993; Destexhe and Sejnowski, 2003). The temporal parameters of propagating and oscillation signals  
513 in our model also matched some of those previously reported: the mean signal propagation velocity and  
514 oscillation frequency measured across homogeneous networks fell within the ranges of spindle wave  
515 propagation velocities and intraspindle spike frequencies reported in both physiological and  
516 computational spindle wave studies (Andersen and Andersson, 1968; Steriade and Deschênes, 1984; Kim  
517 et al., 1995; Destexhe et al., 1996a; Golomb et al., 1996).

518

519 The TC neurons in our model network exhibited both tonic and bursting modes of firing, consistent with  
520 extensive physiological characterization (Sherman, 2001). The form of signal propagation generated in  
521 our networks via open-loop TC-TRN-TC synaptic pathways, which necessarily depended on TRN-driven  
522 post-inhibitory rebound in the downstream TC neuron, could, in practice, be elicited regardless of  
523 whether the upstream TC neuron fired tonically or in bursts. However, bursting in thalamic neurons  
524 receiving open-loop inhibition from the TRN is associated with a greater fidelity of transmission to the

525 cortex relative to tonic firing, as was systematically demonstrated in the computational model that directly  
526 inspired our present study (Willis et al., 2015); this finding furthermore holds relative to thalamocortical  
527 signaling efficiency more generally (Guido et al., 1995; Reinagel et al., 1999, Swadlow and Gusev, 2001;  
528 Krahe and Gabbiani, 2004).

529

530 One particularly notable point of departure relative to similar network models was the extent to which  
531 thalamoreticular, reticulothalamic, and thalamocortical synapses diverged. Although all three classes of  
532 synapses are known to diverge significantly and have been observed to target neuronal somata hundreds  
533 of microns from their origins (Jones, 1985; Cox et al., 1996, 1997; Crabtree, 1996; Pinault and  
534 Deschênes, 1998; Alonso et al., 2001; Miller et al., 2001; Sherman and Guillery, 2001), the TC-TRN,  
535 TRN-TC, and TC-Co synapses in our model were constrained to remain strictly local and minimally  
536 divergent (or non-divergent, in the case of TC-TRN and TC-Co synapses). With respect to the first two  
537 classes of synapses, this constraint was imposed to probe the impact the disynaptic TC-TRN-TC open-  
538 loop motifs characterizing a subset of network permutations, which constituted one of the foci of our  
539 study, and analyze the signal propagation they may support. This neuroanatomical scheme contrasted  
540 with previous computational models featuring parallel, interconnected thalamoreticular pathways, in  
541 which both TC and TRN synapsed bidirectionally with several neighboring TRN and TC cells,  
542 respectively, within a radius of several hundred microns (e.g., Destexhe et al., 1996a, 1998; Golomb et  
543 al., 1996; Bazhenov et al., 1998; Sohal and Huguenard, 1998; Sohal et al., 2000; Traub et al., 2005;  
544 Izhikevich and Edelman, 2008). Furthermore, the limited synaptic divergence constrained the spatial and  
545 temporal scales over which propagating and oscillating signals persisted in our model. This does not  
546 necessarily imply that thalamic and/or cortical signal propagation mediated through open-loop TC-TRN-  
547 TC architectures would be inherently limited in either distance or duration, particularly when accounting  
548 for the comparative diversity and complexity in the spatial and temporal profiles of real sensory  
549 information integrated by the thalamus relative to the highly focal, time-fixed external stimulus  
550 approximations we employed to initialize responses reliably across simulations in our model networks,

551 consistent with similarly simplified stimulus representations utilized in other thalamic or thalamocortical  
552 models (Destexhe et al., 1996a; Golomb et al., 1996; Bazhenov et al., 1998; Sohal and Huguenard, 1998;  
553 Traub et al., 2005). In light of the limits on the spatiotemporal coherence of signals intrinsic to our present  
554 model, however, we would not predict any qualitative changes in propagative or oscillatory dynamics  
555 were we to increase the length of our baseline network as presently constituted by adding in parallel  
556 additional TC, TRN, and Co neurons.

557

558 *The functional implications of open-loop thalamo-reticulo-thalamic synaptic motifs*

559 The spread of activity from one cortical region to another is a foundational concept at the core of our  
560 understanding of sensory processing, higher-order cognitive functions such as attention and language,  
561 sleep-related oscillatory phenomena, and pathological findings such as propagation of ictal discharges and  
562 migraine. It has long been speculated that the TRN could serve as a control point for large-scale cortical  
563 signal processing given its central location, the high degree of convergence of projections involved in  
564 attention, arousal, and emotion onto the TRN, and the TRN's particularly strong control over TC firing  
565 properties (Yingling and Skinner, 1976; Crick, 1984; Guillery et al., 1998; Brunia and Van Boxtel, 2001;  
566 McAlonan et al., 2006; John et al., 2013). Here we showed that open-loop TC-TRN-TC architectures can  
567 support at least short-range thalamocortical signal propagation. Within the thalamus, these configurations  
568 have thus far been observed both within and across individual thalamic nuclei and are thought to serve as  
569 pathways for intra- and cross-modal modulation, respectively (Crabtree et al., 1998; Pinault and  
570 Deschênes, 1998; Crabtree and Isaac, 2002; Lam and Sherman, 2005, 2015; Kimura et al., 2007; Lee et  
571 al., 2010; Kimura, 2014); as has been previously surmised, these synaptic pathways could also plausibly  
572 lend themselves to sensory enhancement, multisensory integration, and attentional mechanisms (Crabtree  
573 and Isaac, 2002; Pinault, 2004; Willis et al., 2015; Crabtree, 2018). At a minimum, and as inferred from  
574 physiological studies, open-loop pathways should be fully capable of supporting signaling propagation  
575 from one thalamic relay neuron to another through a limited number of intervening synapses (with a  
576 disynaptic pathway serving as the shortest such configuration).

577

578 It should be emphasized that the specific functional roles of open-loop TC-TRN-TC pathways are likely  
579 to depend on their densities and distributions within the thalamus (Halassa and Acsády, 2016). If the  
580 morphological, intrinsic, and synaptic heterogeneity of TRN neurons are any indication (Scheibel and  
581 Scheibel, 1966; Jones, 1975; Spreafico et al., 1991; Cox et al., 1996; Lee et al., 2007; Halassa et al., 2014;  
582 Clemente-Perez et al., 2017), it is reasonable to assume that both TC-TRN and TRN-TC synapses are  
583 distributed in a broadly heterogeneous manner across the thalamus. As underscored by our analysis, such  
584 synaptic heterogeneity is seemingly a prerequisite for the propagation of oscillatory signals, which, in the  
585 case of spindling, can occur in the thalamus independently of cortical involvement (von Krosigk et al.,  
586 1993; Bal et al., 1995; Kim et al., 1995) and necessarily involves both recurrently and laterally projecting  
587 TRN-TC synapses, the latter of which form the basis of open loops; outside of this particular functional  
588 context, synaptic heterogeneity is broadly speculated to improve the versatility, efficiency, speed, and  
589 metabolic economy associated with signal processing (Lengler et al., 2013). If open-loop TC-TRN-TC  
590 architectures are indeed to be found within a larger, synaptically diverse thalamoreticular milieu,  
591 characterized by variable synaptic divergence and differing densities of sensory, cortical, and other  
592 extrinsic innervation, it is moreover reasonable to expect that the degree to which the mode of  
593 propagation mediated by these synaptic motifs prevails would vary across thalamic and cortical regions.

594

595 To what extent might the functionality of open loops between the dorsal thalamus and TRN depend on  
596 arousal state? While sleep and other depressed states of consciousness (e.g., those pharmacologically  
597 induced) are associated with thalamic hyperpolarization and therefore tend to amplify both post-inhibitory  
598 rebound, which underlay the signal propagation in our model, and, by extension, low-threshold bursting  
599 (Steriade et al., 1993; McCormick and Bal, 1997; Weyand et al., 2001; Urbain et al., 2019), both  
600 phenomena have also been documented in the thalamic relay neurons of awake animals (Guido and  
601 Weyand, 1995; Fanselow et al., 2001; Ortuño et al., 2014), and then sometimes selectively in response to  
602 particular stimuli (Lesica and Stanley, 2004; Wang et al., 2007). Thus, while there is no mechanistic basis

603 on which to assume that propagation through open TC-TRN-TC loops would be restricted to a particular  
604 state of wakefulness, the widespread modulatory afferents received by both the thalamus and TRN from  
605 brain areas including the prefrontal cortex, basal forebrain, amygdala, and brainstem leave little doubt that  
606 any form of intrathalamic or cortical signaling supported by these synaptic architectures is highly state-  
607 dependent (see, for example, Halassa et al., 2014). Both forthcoming physiological investigation and  
608 future modeling studies will be able to evaluate such predictions and help provide a full accounting of the  
609 role of the various modes of connectivity between brain regions.

610

611 **References:**

612 Ahlsén, G, Lindström, S (1982) Mutual inhibition between perigeniculate neurones. *Brain Res* 236:482-  
613 486.

614

615 Alonso JM, Usrey WM, Reid RC (2001) Rules of connectivity between geniculate cells and simple cells  
616 in cat primary visual cortex. *J Neurosci* 21:4002-4015.

617

618 Andersen P, Andersson SA (1968) The physiological basis of the alpha rhythm. New York: Appleton-  
619 Century-Crofts.

620

621 Asanuma C, Porter LL (1990) Light and electron microscopic evidence for a GABAergic projection from  
622 the caudal basal forebrain to the thalamic reticular nucleus in rats. *J Comp Neurol* 302:159-172.

623

624 Bal T, von Krosigk M, McCormick DA (1995) Role of the ferret perigeniculate nucleus in the generation  
625 of synchronized oscillations in vitro. *J Physiol* 483:665-685.

626

627 Bazhenov M, Timofeev I, Steriade M, Sejnowski TJ (1998) Computational models of thalamocortical  
628 augmenting responses. *J Neurosci* 18:6444-6465.

629  
630 Bazhenov M, Timofeev I, Steriade M, Sejnowski TJ (2002) Model of thalamocortical slow-wave sleep  
631 oscillations and transitions to activated states. *J Neurosci* 22:8691–8704.  
632  
633 Bickford ME, Günlük AE, Van Horn SC, Sherman SM (1994) GABAergic projection from the basal  
634 forebrain to the visual sector of the thalamic reticular nucleus in the cat. *J Comp Neurol* 348:481-510.  
635  
636 Blumenfeld H, McCormick DA (2000) Corticothalamic inputs control the pattern of activity generated in  
637 thalamocortical networks. *J Neurosci* 20:5153-5162.  
638  
639 Brunia CH, Van Boxtel GJ (2001) Wait and see. *Int J Psychophysiol* 43:59-75.  
640  
641 Chen C, Regehr WG (2003) Presynaptic modulation of the retinogeniculate synapse. *J Neurosci*  
642 23:3130-3135.  
643  
644 Clemente-Perez A, Makinson SR, Higashikubo B, Brovarney S, Cho, FS, Urry A, Holden SS, Wimer, M,  
645 Dávid C, Fenno LE, Acsády L, Deisseroth K, Paz JT (2017) Distinct Thalamic Reticular Cell Types  
646 Differentially Modulate Normal and Pathological Cortical Rhythms. *Cell Rep* 19:2130-2142.  
647  
648 Contreras D, Curró Dossi R, Steriade, M (1993) Electrophysiological properties of cat reticular thalamic  
649 neurones in vivo. *J Physiol* 470:273-294.  
650  
651 Contreras D, Destexhe A, Sejnowski TJ, Steriade M (1996) Control of spatiotemporal coherence of a  
652 thalamic oscillation by corticothalamic feedback. *Science* 274:771-774.  
653

- 654 Contreras D, Steriade M (1996) Spindle oscillation in cats: the role of corticothalamic feedback in a  
655 thalamically generated rhythm. *J Physiol* 490:159-179.
- 656
- 657 Cox CL, Huguenard JR, Prince DA (1996) Heterogeneous axonal arborizations of rat thalamic reticular  
658 neurons in the ventrobasal nucleus. *J Comp Neuro* 366:416-430.
- 659
- 660 Cox CL, Huguenard JR, Prince DA (1997) Nucleus reticularis neurons mediate diverse inhibitory effects  
661 in thalamus. *Proc Natl Acad Sci USA* 94:8854-8859.
- 662
- 663 Crabtree JW (1996) Organization in the somatosensory sector of the cat's thalamic reticular nucleus. *J*  
664 *Comp Neurol* 366:207-222.
- 665
- 666 Crabtree JW (2018) Functional Diversity of Thalamic Reticular Subnetworks. *Front Syst Neurosci* 12:41.  
667 doi:10.3389/fnsys.2018.00041
- 668
- 669 Crabtree JW, Collingridge GL, Isaac JT (1998) A new intrathalamic pathway linking modality-related  
670 nuclei in the dorsal thalamus. *Nat Neurosci* 1:389-394.
- 671
- 672 Crabtree JW, Isaac JT (2002) New intrathalamic pathways allowing modality-related and cross-modality  
673 switching in the dorsal thalamus. *J Neurosci* 22:8754-8761.
- 674
- 675 Crandall SR, Cruikshank SJ, Connors BW (2015) A corticothalamic switch: controlling the thalamus with  
676 dynamic synapses. *Neuron* 86:768-782.
- 677
- 678 Crandall SR, Govindaiah G, Cox CL (2010) Low-threshold  $\text{Ca}^{2+}$  current amplifies distal dendritic  
679 signaling in thalamic reticular neurons. *J Neurosci* 30:15419-15429.

680

681 Crick F (1984) Function of the thalamic reticular complex: the searchlight hypothesis. *Proc Natl Acad Sci*  
682 *USA* 81:4586-4590.

683

684 Cruikshank SJ, Urabe H, Nurmikko AV, Connors BW (2010) Pathway-specific feedforward circuits  
685 between thalamus and neocortex revealed by selective optical stimulation of axons. *Neuron* 65:230-245.

686

687 Dayan P, Abbott LF (2005) *Theoretical Neuroscience*, revised edition. Cambridge, MA: MIT Press.

688

689 De Curtis M, Spreafico R, Avanzini G (1989) Excitatory amino acids mediate responses elicited in vitro  
690 by stimulation of cortical afferents to reticularis thalami neurons of the rat. *Neuroscience* 33:275-283.

691

692 Deleuze C, Huguenard (2006) Distinct electrical and chemical connectivity maps in the thalamic reticular  
693 nucleus: potential roles in synchronization and sensation. *J Neurosci* 26:8633-8645.

694

695 Deleuze C, David F, Béhuret S, Sadoc G, Shin HS, Uebele VN, Renger JJ, Lambert RC, Leresche N, Bal  
696 T (2012) T-type calcium channels consolidate tonic action potential output of thalamic neurons to  
697 neocortex. *J Neurosci* 32:12228–12236.

698

699 Destexhe A, Bal T, McCormick DA, Sejnowski TJ (1996a) Ionic mechanisms underlying synchronized  
700 oscillations and propagating waves in a model of ferret thalamic slices. *J Neurophysiol* 76:2049-2070.

701

702 Destexhe A, Contreras D, Steriade M (1998) Mechanisms underlying the synchronizing action of  
703 corticothalamic feedback through inhibition of thalamic relay cells. *J Neurophysiol* 79:999–1016.

704

- 705 Destexhe A, Contreras D, Steriade M, Sejnowski TJ, Huguenard JR (1996b) In vivo, in vitro, and  
706 computational analysis of dendritic calcium currents in thalamic reticular neurons. *J Neurosci* 16:169-  
707 185.
- 708
- 709 Destexhe A, McCormick DA, Sejnowski TJ (1993) A model for 8–10 Hz spindling in interconnected  
710 thalamic relay and reticularis neurons. *Biophys J* 65:2473–2477.
- 711
- 712 Destexhe A, Sejnowski TJ (2003) Interactions between membrane conductances underlying  
713 thalamocortical slow-wave oscillations. *Physiol Rev* 83:1401-1453.
- 714
- 715 Dong P, Wang H, Shen X-F, Jiang P, Zhu X-T, Li Y, Gao J-H, Lin S, Huang Y, He X-B, Xu FQ, Duan S,  
716 Lian H, Wang H, Chen J, Li XM (2019) A novel cortico-intrathalamic circuit for flight behavior. *Nat*  
717 *Neurosci* 22:941-949.
- 718
- 719 Fanselow EE, Sameshima K, Baccala LA, Nicolelis MA (2001) Thalamic bursting in rats during different  
720 awake behavioral states. *Proc Natl Acad Sci USA* 98:15330–15335.
- 721
- 722 Felleman DJ, Van Essen DC (1991) Distributed hierarchical processing in the primate cerebral cortex.  
723 *Cereb Cortex* 1:1-47.
- 724
- 725 Ferrarelli F, Tononi G (2011) The thalamic reticular nucleus and schizophrenia. *Schizophr Bull* 37:306-  
726 315.
- 727
- 728 FitzGibbon T, Solomon SG, Goodchild AK (2000) Distribution of calbindin, parvalbumin, and calretinin  
729 immunoreactivity in the reticular thalamic nucleus of the marmoset: evidence for a medial leaflet of  
730 incertal neurons. *Exp Neurol* 164:371-383.

731  
732 Friedman J, Hastie J, Tibshirani R (2010) Regularization paths for generalized linear models via  
733 coordinate descent. *J Stat Softw* 33:1-22.  
734  
735 Fuentealba P, Crochet S, Timofeev I, Bazhenov M, Sejnowski TJ, Steriade M (2004) Experimental  
736 evidence and modeling studies support a synchronizing role for electrical coupling in the cat thalamic  
737 reticular neurons in vivo. *Eur J Neurosci* 20:111-119.  
738  
739 Gentet LJ, Ulrich D (2003) Strong, reliable and precise synaptic connections between thalamic relay cells  
740 and neurones of the nucleus reticularis in juvenile rats. *J Physiol* 546:801-811.  
741  
742 Golomb D, Wang XJ, Rinzel J (1996) Propagation of spindle waves in a thalamic slice model. *J*  
743 *Neurophysiol* 75:750-769.  
744  
745 Guido W, Lu SM, Vaughan J, Godwin DW, Sherman SM (1995) Receiver operating characteristic (ROC)  
746 analysis of neurons in the cat's lateral geniculate nucleus during tonic and burst response mode. *Vis*  
747 *Neurosci* 12:723-741.  
748  
749 Guido W, Weyand T (1995) Burst responses in thalamic relay cells of the awake behaving cat. *J*  
750 *Neurophysiol* 74:1782-1786.  
751  
752 Guillery RW, Feig SL, Lozsádi DA (1998) Paying attention to the thalamic reticular nucleus. *Trends*  
753 *Neurosci* 21:28-32.  
754  
755 Halassa MM, Acsády L (2016) Thalamic inhibition: diverse sources, diverse scales. *Trends Neurosci*  
756 39:680-693.

757

758 Halassa MM, Chen Z, Wimmer RD, Brunetti PM, Zhao S, Zikopoulos B, Wang F, Brown EN, Wilson  
759 MA (2014) State-dependent architecture of thalamic reticular subnetworks. *Cell* 158:808-821.

760

761 Hale PT, Sefton AJ, Bauer LA, Cottee LJ (1982) Interrelations of the rat's thalamic reticular and dorsal  
762 lateral geniculate nuclei. *Exp Brain Res* 45:217-229.

763

764 Hallanger AE, Levey AI, Lee HJ, Rye DB, Wainer BH (1987) The origins of cholinergic and other  
765 subcortical afferents to the thalamus in the rat. *J Comp Neurol* 262:105-124.

766

767 Herz AV, Gollisch T, Machens CK, Jaeger D (2006) Modeling single-neuron dynamics and  
768 computations: a balance of detail and abstraction. *Science* 314:80-85.

769

770 Hou G, Smith AG, Zhang ZW (2016) Lack of intrinsic GABAergic connections in the thalamic reticular  
771 nucleus of the mouse. *J Neurosci* 36:7246-7252.

772

773 Huguenard JR (1998) Neuronal circuitry of thalamocortical epilepsy and mechanisms of antiabsence drug  
774 action. *Adv Neurol* 79:991-999.

775

776 Izhikevich EM, Edelman GM (2008) Large-scale model of mammalian thalamocortical systems. *Proc*  
777 *Natl Acad Sci USA* 105:3593-3598.

778

779 John YJ, Bullock D, Zikopoulos B, Barbas H (2013) Anatomy and computational modeling of networks  
780 underlying cognitive-emotional interaction. *Front Hum Neurosci* 7:101.

781

782 Jones EG (1975) Some aspects of the organization of the thalamic reticular complex. *J Comp Neurol*  
783 162:285-308.  
784  
785 Jones EG (1985) *The Thalamus*. New York: Plenum Press.  
786  
787 Kim U, Bal T, McCormick DA (1995) Spindle waves are propagating synchronized oscillations in the  
788 ferret LGNd in vitro. *J Neurophysiol* 74:1301-1323.  
789  
790 Kimura A (2014) Diverse subthreshold cross-modal sensory interactions in the thalamic reticular nucleus:  
791 implications for new pathways of cross-modal attentional gating function. *Eur J Neurosci* 39:1405-1418.  
792  
793 Kimura A, Imbe H, Donishi T, Tamai Y (2007) Axonal projections of single auditory neurons in the  
794 thalamic reticular nucleus: implications for tonotopy-related gating function and cross-modal modulation.  
795 *Eur J Neurosci* 26:3524-3535.  
796  
797 Kokkinos V, Koupparis AM, Koutroumanidis M, Kostopoulos GK (2017) Spatiotemporal propagation  
798 patterns of generalized ictal spikes in childhood absence epilepsy *Clin Neurophysiol* 128:1553-1562.  
799  
800 Kötter R, Sommer FT (2000) Global relationship between anatomical connectivity and activity  
801 propagation in the cerebral cortex. *Philos Trans R Soc Lond, B, Biol Sci* 355:127-134.  
802  
803 Krahe R, Gabbiani F (2004) Burst firing in sensory systems. *Nat Rev Neurosci* 5:13-23.  
804  
805 Krol A, Wimmer RD, Halassa MM, Feng G (2018) Thalamic reticular dysfunction as a circuit  
806 endophenotype in neurodevelopmental disorders. *Neuron* 98:282-295.  
807

- 808 Lam YW, Sherman SM (2005) Mapping by laser photostimulation of connections between the thalamic  
809 reticular and ventral posterior lateral nuclei in the rat. *J Neurophysiol* 94:2472–2483.  
810
- 811 Lam YW, Sherman SM (2015) Functional topographic organization of the motor reticulothalamic  
812 pathway. *J Neurophysiol* 113:3090-3097.  
813
- 814 Lam, YW, Nelson CS, Sherman SM (2006) Mapping of the functional interconnections between thalamic  
815 reticular neurons using photostimulation. *J Neurophysiol* 96:2593–2600.  
816
- 817 Landisman CE, Long MA, Beierlein M, Deans MR, Paul DL, Connors BW (2002) Electrical synapses in  
818 the thalamic reticular nucleus. *J Neurosci* 22:1002–1009.  
819
- 820 Leao AAP (1944) Spreading depression of activity in the cerebral cortex. *J Neurophysiol* 7:359–390.  
821
- 822 Lee SC, Cruikshank SJ, Connors BW (2010) Electrical and chemical synapses between relay neurons in  
823 developing thalamus. *J Physiol* 588:2403-2415.  
824
- 825 Lee SH, Govindaiah G, Cox CL (2007) Heterogeneity of firing properties among rat thalamic reticular  
826 nucleus neurons. *J Physiol (Lond)* 582:195-208.  
827
- 828 Lengler J, Jug F, Steger A (2013) Reliable neuronal systems: the importance of heterogeneity. *PLoS One*  
829 8:e80694.  
830
- 831 Lesica NA, Stanley GB (2004) Encoding of natural scene movies by tonic and burst spikes in the lateral  
832 geniculate nucleus. *J Neurosci* 24:10731-10740.  
833

- 834 Llinás RR, Paré D (1991) Of dreaming and wakefulness. *Neuroscience* 44:521-535.  
835
- 836 Lo FS, Sherman SM (1994) Feedback inhibition in the cat's lateral geniculate nucleus. *Exp Brain Res*  
837 100:365-368.  
838
- 839 Long MA, Landisman CE, Connors BW (2004) Small clusters of electrically coupled neurons generate  
840 synchronous rhythms in the thalamic reticular nucleus. *J Neurosci* 24:341-349.  
841
- 842 McAlonan K, Cavanaugh J, Wurtz RH (2006) Attentional modulation of thalamic reticular neurons. *J*  
843 *Neurosci* 26:4444-4450.  
844
- 845 McCormick DA, Bal T (1997) Sleep and arousal: thalamocortical mechanisms. *Annu Rev Neurosci*  
846 20:185-215.  
847
- 848 McCormick DA, Contreras D (2001) On the cellular and network bases of epileptic seizures. *Annu Rev*  
849 *Physiol* 63:815-846.  
850
- 851 McCormick DA, Pape HC (1980) Properties of a hyperpolarization-activated cation current and its role in  
852 rhythmic oscillation in thalamic relay neurones. *J Physiol (Lond)* 431:291-318.  
853
- 854 Miller LM, Escabí MA, Read HL, Schreiner CE (2001) Functional convergence of response properties in  
855 the auditory thalamocortical system. *Neuron* 32:151-160.  
856
- 857 Moore JW, Ramon F (1974) On numerical integration of the Hodgkin and Huxley equations for a  
858 membrane action potential. *J Theor Biol* 45:249-273.  
859

- 860 Morrison JH, Foote SL (1986) Noradrenergic and serotonergic innervation of cortical, thalamic, and  
861 tectal visual structures in Old and New World monkeys. *J Comp Neurol* 243:117-138.  
862
- 863 Muller L, Chavane F, Reynolds J, Sejnowski TJ (2018) Cortical travelling waves: mechanisms and  
864 computational principles. *Nat Rev Neurosci* 19:255-268.  
865
- 866 Muller L, Piantoni G, Koller D, Cash SS, Halgren E, Sejnowski, TJ (2016) Rotating waves during human  
867 sleep spindles organize global patterns of activity that repeat precisely through the night. *eLife* 5:e17267.  
868
- 869 Muller L, Reynaud A, Chavane F, Destexhe A (2014) The stimulus-evoked population response in visual  
870 cortex of awake monkey is a propagating wave. *Nat Commun* 5:3675.  
871
- 872 Ortuño T, Grieve KL, Cao R, Cudeiro J, Rivadulla C (2014) Bursting thalamic responses in awake  
873 monkey contribute to visual detection and are modulated by corticofugal feedback. *Front Behav Neurosci*  
874 8:198.  
875
- 876 Parent A, Hazrati LN (1995) Functional anatomy of the basal ganglia. I. The cortico-basal ganglia-  
877 thalamo-cortical loop. *Brain Res Brain Res Rev* 20:91-127.  
878
- 879 Pham T, Haas JS (2018) Electrical synapses between inhibitory neurons shape the responses of principal  
880 neurons to transient inputs in the thalamus: a modeling study. *Sci Rep* 8:7763.  
881
- 882 Pinault D (2004) The thalamic reticular nucleus: structure, function and concept. *Brain Res Brain Res Rev*  
883 46:1-31.  
884

- 885 Pinault D, Deschênes M (1998) Anatomical evidence for a mechanism of lateral inhibition in the rat  
886 thalamus. *Eur J Neurosci* 10:3462-3469.
- 887
- 888 Pinault D, Smith Y, Deschênes M (1997) Dendrodendritic and axoaxonic synapses in the thalamic  
889 reticular nucleus of the adult rat. *J Neurosci* 17:3215-3233.
- 890
- 891 Pita-Almenar JD, Yu D, Lu HC, Beierlein M (2014) Mechanisms underlying desynchronization of  
892 cholinergic-evoked thalamic network activity. *J Neurosci* 34:14463–14474.
- 893
- 894 Pospischil M, Toledo-Rodriguez M, Monier C, Piwkowska Z, Bal T, Frégnac Y, Markram H, Destexhe A  
895 (2008) Minimal Hodgkin-Huxley type models for different classes of cortical and thalamic neurons. *Biol*  
896 *Cybern* 99:427–441.
- 897
- 898 R Core Team (2013) R: A language and environment for statistical computing (R Foundation for  
899 Statistical Computing, Vienna). URL <http://www.R-project.org/>.
- 900
- 901 Reinagel P, Godwin D, Sherman SM, Koch C (1999) Encoding of visual information by LGN bursts. *J*  
902 *Neurophysiol* 81:2558-2569.
- 903
- 904 Rogala J, Waleszczyk WJ, Łęski S, Wróbel A, Wójcik DK (2013) Reciprocal inhibition and slow calcium  
905 decay in perigeniculate interneurons explain changes of spontaneous firing of thalamic cells caused by  
906 cortical inactivation. *J Comput Neurosci* 34:461-476.
- 907
- 908 Roy JP, Clercq M, Steriade M, Deschênes M (1984) Electrophysiology of neurons of lateral thalamic  
909 nuclei in cat: mechanisms of long-lasting hyperpolarizations. *J Neurophysiol* 51:1220-1235.
- 910

- 911 Sanchez-Vives, MV, Bal T, McCormick DA (1997) Inhibitory interactions between perigeniculate  
912 GABAergic neurons. *J Neurosci* 17:8894-8908.  
913
- 914 Scheibel ME, Scheibel AB (1966) The organization of the nucleus reticularis thalami: a Golgi study.  
915 *Brain Res* 1:43-62.  
916
- 917 Sherman SM (2001) Tonic and burst firing: dual modes of thalamocortical relay. *Trends Neurosci*  
918 24:122-126.  
919
- 920 Sherman SM, Guillery RW (1996) Functional organization of thalamocortical relays. *J Neurophysiol*  
921 76:1367-1395.  
922
- 923 Sherman SM, Guillery RW (2001) Exploring the thalamus. San Diego: Academic Press.  
924
- 925 Shimizu K, Stopfer M (2013) Gap junctions. *Curr Biol* 23:R1026-1031.  
926
- 927 Shosaku A (1986) Cross-correlation analysis of a recurrent inhibitory circuit in the rat thalamus. *J*  
928 *Neurophysiol* 55:1030-1043.  
929
- 930 Shu Y, McCormick DA (2002) Inhibitory interactions between ferret thalamic reticular neurons. *J*  
931 *Neurophysiol* 87:2571-2576.  
932
- 933 Siegel A, Sapru HN (2015) Essential Neuroscience, Third Edition. Baltimore: Lippincott Williams &  
934 Wilkins.  
935

- 936 Sillito AM, Cudeiro J, Jones HE (2006) Always returning: feedback and sensory processing in visual  
937 cortex and thalamus. *Trends Neurosci* 29:307-316.  
938
- 939 Sohal VS, Huguenard JR (1998) Long-range connections synchronize rather than spread intrathalamic  
940 oscillations: computational modeling and in vitro electrophysiology. *J Neurophysiol* 80:1736-1751.  
941
- 942 Sohal VS, Huntsman MM, Huguenard JR (2000) Reciprocal inhibitory connections regulate the  
943 spatiotemporal properties of intrathalamic oscillations. *J Neurosci* 20:1735-1745.  
944
- 945 Sorokin JM, Davidson TJ, Frechette E, Abramian AM, Deisseroth K, Huguenard JR, Paz JT (2017)  
946 Bidirectional control of generalized epilepsy networks via rapid real-time switching of firing mode.  
947 *Neuron* 93:194-210.  
948
- 949 Spreafico R, Battaglia G, Frassoni C (1991) The reticular thalamic nucleus (RTN) of the rat:  
950 cytoarchitectural, Golgi, immunocytochemical, and horseradish peroxidase study. *J Comp Neurol*  
951 304:478-90.  
952
- 953 Steriade M, Deschênes M (1984) The thalamus as a neuronal oscillator. *Brain Res* 320:1-63.  
954
- 955 Steriade M, Jones EG, Llinás RR (1990) *Thalamic Oscillations and Signaling*. New York: Wiley-  
956 Interscience.  
957
- 958 Steriade M, McCormick D, Sejnowski T (1993) Thalamocortical oscillations in the sleeping and aroused  
959 brain. *Science* 262:679-685.  
960

- 961 Steriade M, Wyzinski P, Apostol V (1972) Corticofugal projections governing rhythmic thalamic  
962 activity. In: Corticothalamic Projections and Sensorimotor Activities (Frigyesi TL, Rinvik E, Yahr MD,  
963 eds), pp 221-272. New York: Raven.  
964
- 965 Suga N, Ma X (2003) Multiparametric corticofugal modulation and plasticity in the auditory system. *Nat*  
966 *Rev Neurosci* 4:783-794.  
967
- 968 Sun, YG, Pita-Almenar JD, Wu CS, Renger JJ, Uebele VN, Lu HC, Beierlein M (2013) Biphasic  
969 cholinergic synaptic transmission controls action potential activity in thalamic reticular nucleus neurons. *J*  
970 *Neurosci* 33:2048–2059.  
971
- 972 Swadlow H, Gusev A (2001) The impact of “bursting” thalamic impulses at a neocortical synapse. *Nat*  
973 *Neurosci* 4:402-408.  
974
- 975 Theyel BB, Llano DA, Sherman SM (2010) The corticothalamocortical circuit drives higher-order cortex  
976 in the mouse. *Nat Neurosci* 13:84-88.  
977
- 978 Traub RD, Contreras D, Cunningham MO, Murray H, LeBeau FE, Roopun A, Bibbig A, Wilentz WB,  
979 Higley MJ, Whittington MA (2005) Single-column thalamocortical network model exhibiting gamma  
980 oscillations, sleep spindles, and epileptogenic bursts. *J Neurophysiol* 93:2194-2232.  
981
- 982 Tsodyks MV, Markram H (1997) The neural code between neocortical pyramidal neurons depends on  
983 neurotransmitter release probability. *Proc Natl Acad Sci USA* 94:719–723.  
984

- 985 Urbain N, Fourcaud-Trocmé N, Laheux S, Salin PA, Gentet LJ (2019) Brain-state-dependent modulation  
986 of neuronal firing and membrane potential dynamics in the somatosensory thalamus during natural sleep.  
987 *Cell Reports* 26:1443-1457.
- 988
- 989 von Krosigk, M, Bal T, McCormick DA (1993) Cellular mechanisms of a synchronized oscillation in the  
990 thalamus. *Science* 261:361-364.
- 991
- 992 Wang X, Wei Y, Vaingankar V, Wang Q, Koepsell K, Sommer FT, Hirsch JA (2007) Feedforward  
993 excitation and inhibition evoke dual modes of firing in the cat's visual thalamus during naturalistic  
994 viewing. *Neuron* 55:465-478.
- 995
- 996 Warren RA, Agmon A, Jones EG (1994) Oscillatory synaptic interactions between ventroposterior and  
997 reticular neurons in mouse thalamus in vitro. *J Neurophysiol* 72:1993-2003.
- 998
- 999 Wells MF, Wimmer RD, Schmitt LI, Feng G, Halassa MM (2016) Thalamic reticular impairment  
1000 underlies attention deficit in *Ptchd1*(Y/-) mice. *Nature* 532:58-63.
- 1001
- 1002 Weyand TG, Boudreaux M, Guido W (2001) Burst and tonic response modes in thalamic neurons during  
1003 sleep and wakefulness. *J Neurophysiol* 85:1107-1118.
- 1004
- 1005 White EL, Hersch SM (1982) A quantitative study of thalamocortical and other synapses involving the  
1006 apical dendrites of corticothalamic projection cells in mouse Sml cortex. *J Neurocytol* 11:137-157.
- 1007
- 1008 Williams SR, Stuart GJ (2000) Action potential backpropagation and somato-dendritic distribution of ion  
1009 channels in thalamocortical neurons. *J Neurosci* 20:1307-1317.
- 1010

- 1011 Willis AM, Slater BJ, Gribkova ED, Llano DA (2015) Open-loop organization of thalamic reticular  
1012 nucleus and dorsal thalamus: a computational model. *J Neurophysiol* 114:2353-2367.  
1013
- 1014 Wimmer RD, Schmitt LI, Davidson TJ, Nakajima M, Deisseroth K, Halassa MM (2015) Thalamic control  
1015 of sensory selection in divided attention. *Nature* 526:705-709.  
1016
- 1017 Yamada WM, Koch C, Adams PR (1989) Multiple channels and calcium dynamics. In: *Methods in*  
1018 *Neuronal Modeling* (Koch C, Segev I, eds), pp 97–133. Cambridge, MA: MIT Press.  
1019
- 1020 Yingling CD, Skinner JE (1976) Selective regulation of thalamic sensory relay nuclei by nucleus  
1021 reticularis thalami. *Electroencephalogr Clin Neurophysiol* 41:476-482.  
1022
- 1023 Zhang L, Jones EG (2004) Corticothalamic inhibition in the thalamic reticular nucleus. *J Neurophysiol*  
1024 91:759-766.  
1025
- 1026 Zikopoulos B, Barbas H (2006) Prefrontal projections to the thalamic reticular nucleus form a unique  
1027 circuit for attentional mechanisms. *J Neurosci* 26:7348-7361.

1028 **Figures:**

1029 **Figure 1.** Pathways and properties of thalamocortical signaling. **A:** Closed- vs. open-loop thalamo-  
1030 reticulo-thalamic configurations. **B:** Three possible pathways through which a signal might propagate  
1031 from one thalamocortical (TC) neuron to another via the thalamic reticular nucleus (TRN). **C:** Baseline  
1032 thalamocortical model network. Broken-line synapses were allowed to vary either as a class  
1033 (homogeneously) or independently of one another (heterogeneously). The black arrow corresponds to the  
1034 fixed, external stimulus applied to TC<sub>1</sub>. **D:** Sample cortical (Co) spike histograms (detrended) in a  
1035 network permutation responding to a fixed, sustained stimulus delivered to TC<sub>1</sub> (black bar beneath the  
1036 lowest trace). The propagation score assigned to any network permutation was quantified as the amplitude  
1037 of the initial stimulus-evoked response in the detrended Co<sub>3</sub> histogram; response propagation across the  
1038 cortical subnetwork (orange arrow) was consistently linear, and thus the initial response in Co<sub>3</sub> was  
1039 observed at a fixed interval relative to the onset of stimulation. Oscillation intrinsic to any network variant  
1040 was quantified as the amplitude of the first off-center peak in the normalized autocorrelogram (right) of  
1041 post-stimulation activity in the detrended Co<sub>3</sub> histogram (within broken black box). The initial 400 ms of  
1042 activity preceding the fixed stimulus (in grey) is shown here for each histogram but was not included in  
1043 the calculations of either propagation or oscillation. Note that the bin heights in the Co<sub>1</sub> histogram shown  
1044 here were truncated in order to maintain identical vertical scaling across all three cortical histograms.

1045 **Figure 2.** Propagation and oscillation in homogeneously varied synaptic networks (N=770). **A:** Ordinal  
1046 heat maps ranking homogeneously varied synaptic network permutations according to the extent of  
1047 supported signal propagation and oscillation. Every row in a given map depicts a single network  
1048 permutation, color-coded based on its synaptic makeup according to the three synaptic scales found below  
1049 the maps (redder colors signify stronger or more open-loop connections). The network property ranks and  
1050 synaptic makeups of two selected networks, Networks  $\alpha$  and  $\beta$ , are indicated. **B:** Representative  
1051 simulations and circuit diagrams depicting the normalized synaptic makeups for the two selected  
1052 networks. The yellow arrow indicates when the fixed stimulus was delivered to TC<sub>1</sub> in each simulation.  
1053 Orange highlighting indicates epochs of linear propagation, while circles are placed above spikes  
1054 occurring during periods of oscillatory activity. **C:** Heat maps displaying propagation scores in TRN-  
1055 TRN synaptic parameter space for the 70 fully open-loop networks (openness coefficient=1.0), with  
1056 Network  $\alpha$  highlighted (left), and propagation as a function of TC-TRN-TC openness and electrical  
1057 coupling between TRN neurons for the 70 networks possessing 200-nS GABAergic TRN-TRN synapses  
1058 (right). **D:** Mean oscillation scores for networks varied nonlinearly as a function of their openness  
1059 coefficients, with networks possessing openness coefficients of 0 and 0.4 supporting oscillation to equal  
1060 extents (one-way ANOVA with Tukey post-hoc tests,  $F(10,759)=137.8$ ,  $p<0.0001$ ). Individual means  
1061 were computed by averaging the 70 oscillation scores associated with a given openness coefficients, and  
1062 error bars indicate standard errors of the mean; N.S.=not significant.

1063 **Figure 3.** Propagation and oscillation in heterogeneously varied synaptic networks (N=12,681). **A:**  
1064 Network regression models illustrating how propagation (top) and oscillation (bottom) varied as a  
1065 function of individual synaptic weights across simulated heterogeneously synaptic network permutations.  
1066 Synapses with positive and negative normalized regressions coefficients were correlated positively and  
1067 negatively with a given property and are depicted separately in the left- and right-sided circuit diagrams,  
1068 respectively, for clarity. Gray synapses are either non-variable or associated with normalized regression  
1069 coefficients with absolute values less than 0.05. See also Table 4. **B:** Representative simulations for two  
1070 selected heterogeneous networks, whose normalized synaptic weights are depicted in the circuit diagrams.  
1071 Networks  $\alpha'$  and  $\beta'$  respectively illustrate propagation and propagation of oscillation across the network.

1072 **Figure 4.** Heterogeneously varied synaptic architectures better supported propagation of oscillation.  
1073 Propagation, as measured in those network permutations scoring highest with respect to the property, was  
1074 equally supported in networks where synaptic weights varied independently of one another  
1075 (heterogeneously; checkered) as in networks where synaptic strength varied homogeneously (black) by  
1076 class [unpaired  $t$ -test,  $t(38)=0.46$ ,  $p=0.647$ ]. By contrast, oscillation and optimization scores were  
1077 significantly higher in top-performing heterogeneous networks than their homogeneous counterparts  
1078 [oscillation:  $t(38)=13.88$ ,  $p<0.0001$ ; optimization:  $t(38)=18.04$ ,  $p<0.0001$ ]. Each bar corresponds to a  
1079 mean of the top 20 network propagation or oscillation scores within each synaptic architecture group;  
1080 error bars indicate standard errors of the mean. \*\*\*\*= $p<0.0001$ ; N.S.=not significant.

1081 **Tables:**

Intrinsic Model Cellular Parameters			
Parameter	TC cell	TRN cell	Co cell
Leak conductance, $g_L$ (nS)	3.263	3.7928	4.8128
Leak reversal potential, $E_L$ (mV)	-60.03	-57	-60.2354
Transient sodium conductance, $g_{Na}$ (nS)	1,500	3,000	3,000
Sodium equilibrium potential, $E_{Na}$ (mV)	50		
Delayed-rectifier potassium conductance, $g_K$ (nS)	520	400	140
M-type potassium conductance, $g_M$ (nS)	-	3.5	1.5
M-type potassium time constant, $\tau_M$ (ms)	-	200	180
Potassium equilibrium potential, $E_K$ (mV)	-100		-90
T-type calcium conductance, $g_T$ (nS)	45	21	-
Calcium equilibrium potential, $E_T$ (mV)	120		
H-current conductance, $g_H$ (nS)	0.608	0.0192	-
H-current reversal potential, $E_H$ (mV)	-33		-
Membrane capacitance, $C_m$ (pF)	100.4	75.0	109.3865

1082 **Table 1.** Intrinsic model cellular parameters.

Model Synaptic Parameters						
Synapse	Neurotransmitter	Conductance (nS)	$\tau_{\text{recov}}$ (ms)	$\tau_{\text{inact}}$ (ms)	Reversal Potential (mV)	$U_{SE}$
External synapse to TC cell	(Glutamate)	32	125	2.64	0	0.76
TC-to-TRN cell synapse (TC-TRN)	Glutamate	150	500	2.64	0	0.76
TC-to-Co cell synapse (TC-Co)	Glutamate	50	160	11.52	0	0.8113
TRN-to-TC cell synapse (TRN-TC)	GABA <sub>A</sub>	Variable (0-80)	167.29	16.62	-80	0.62
Chemical TRN-to-TRN cell synapse (TRN-TRN <sub>GABA</sub> )	GABA <sub>A</sub>	Variable (0-450)	225	15	-75	0.62

1083 **Table 2.** Model synaptic parameters.  $\tau_{\text{recov}}$ , synaptic recovery time constant;  $\tau_{\text{inact}}$ , synaptic recovery time  
1084 constant;  $U_{SE}$ , fraction of recovered resources (synaptic vesicles) that can be converted to an active state  
1085 (Tsodyks and Markram, 1997).

Normalized Regression Coefficients for Homogeneously Varied Synaptic Networks				
Synaptic Variable	Propagation	Propagation	Oscillation	Oscillation 2°
	Linear	2°	Linear	
$\text{TRN-TRN}_{\text{GABA}}$	-0.173	-0.670	-	0.060
$\text{TRN-TRN}_{\text{Elec}}$	-0.136	-0.347	-	-
$\text{Open}_{\text{TC-TRN-TC}}$	1.000	1.000	-1.000	-0.052
$(\text{TRN-TRN}_{\text{GABA}})^2$	-	0.332	-	-
$(\text{TRN-TRN}_{\text{Elec}})^2$	-	0.164	-	-
$(\text{Open}_{\text{TC-TRN-TC}})^2$	-	0.594	-	-1.000
$\text{TRN-TRN}_{\text{GABA}} \times \text{TRN-TRN}_{\text{Elec}}$	-	0.262	-	-
$\text{TRN-TRN}_{\text{GABA}} \times \text{Open}_{\text{TC-TRN-TC}}$	-	-0.152	-	-
$\text{TRN-TRN}_{\text{Elec}} \times \text{Open}_{\text{TC-TRN-TC}}$	-	-0.365	-	-

1086

1087 **Table 3.** Normalized linear and second-order regression coefficients for propagation and oscillation in

1088 homogeneously varied synaptic networks. The regressions include 1°, 2°, and interaction terms

1089 corresponding to  $\text{TRN-TRN}_{\text{GABA}}$ ,  $\text{TRN-TRN}_{\text{Elec}}$ , and TC-TRN-TC openness ( $\text{Open}_{\text{TC-TRN-TC}}$ ). Terms1090 associated with regression coefficients of absolute values  $< 0.05$  are omitted. Linear regression for1091 propagation,  $R^2=0.793$ ,  $\text{RMSE}=0.047$ ,  $p<0.0001$ ; second-order regression for propagation,  $R^2=0.842$ ,1092  $\text{RMSE}=0.041$ ,  $p<0.0001$ ; linear regression for oscillation,  $R^2=0.526$ ,  $\text{RMSE}=0.145$ ,  $p<0.0001$ ; second-1093 order regression for oscillation,  $R^2=0.630$ ,  $\text{RMSE}=0.128$ ,  $p<0.0001$ .

Normalized Regression Coefficients in Heterogeneously Varied Synaptic Networks				
Synaptic Variable	Propagation	Propagation	Oscillation	Oscillation
	Linear	2°	Linear	2°
$TRN_1-TRN_3$	-	-	0.115	-
$TRN_3-TRN_1$	-0.088			
$TRN_3-TRN_2$	-0.084	-0.073	-	-
$TRN_1=TRN_2$	-0.051	-0.091	-	-
$TRN_1=TRN_3$	-0.072	-	-	-
$TRN_2=TRN_3$	-	-0.113	0.117	-
$TRN_1-TC_1$	-0.075	-	0.621	0.077
$TRN_1-TC_2$	0.608	0.571	-0.289	-1.000
$TRN_2-TC_2$	-0.128	-0.196	0.333	0.417
$TRN_2-TC_3$	1.000	1.000	-0.379	-0.892
$TRN_3-TC_3$	-0.207	-0.239	1.000	0.107
$(TRN_3-TRN_2)^2$	-	0.079	-	-
$(TRN_1-TC_2)^2$	-	-0.245	-	0.189
$(TRN_2-TC_2)^2$	-	0.174	-	-0.093
$(TRN_2-TC_3)^2$	-	-0.472	-	0.278
$(TRN_3-TC_3)^2$	-	0.187	-	-0.146
$TRN_1-TRN_2 \times TRN_1-TC_2$	-	0.070	-	-
$TRN_1-TRN_3 \times TRN_3-TC_3$	-	-	-	0.215
$TRN_2-TRN_1 \times TRN_1=TRN_2$	-	-	-	0.111
$TRN_2-TRN_1 \times TRN_1-TC_1$	-	-	-	-0.186

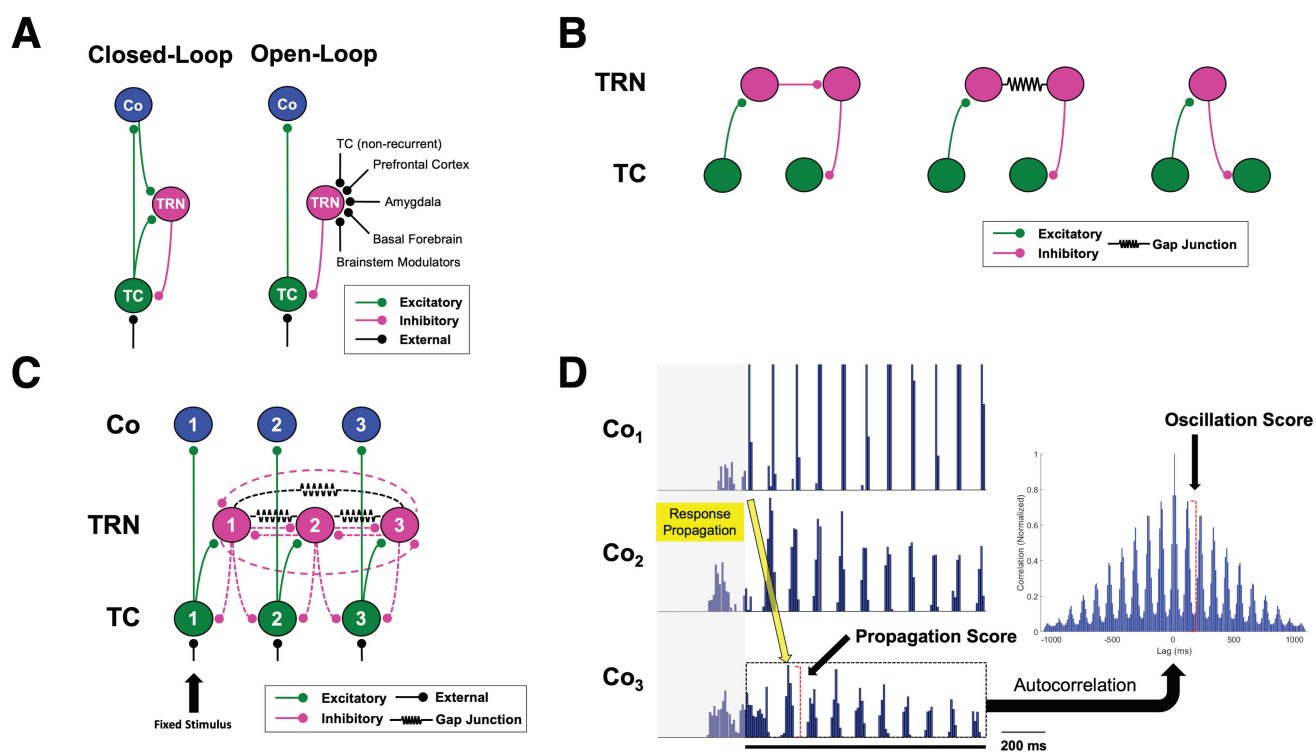
$TRN_3-TRN_1 \times TRN_1-TC_1$	-	-	-	-0.172
$TRN_3-TRN_1 \times TRN_1-TC_2$	-	-0.119	-	-
$TRN_3-TRN_1 \times TRN_2-TC_3$	-	-0.096	-	-
$TRN_3-TRN_2 \times TRN_2-TC_3$	-	-0.153	-	-
$TRN_1=TRN_2 \times TRN_2-TC_3$	-	-	-	-0.129
$TRN_1=TRN_3 \times TRN_1-TC_1$	-	-	-	-0.114
$TRN_1=TRN_3 \times TRN_3-TC_3$	-	-0.079	-	-
$TRN_1-TC_1 \times TRN_1-TC_2$	-	-	-	0.634
$TRN_1-TC_1 \times TRN_2-TC_3$	-	-	-	0.449
$TRN_1-TC_2 \times TRN_2-TC_2$	-	-0.166	-	0.361
$TRN_1-TC_2 \times TRN_2-TC_3$	-	0.753	-	-0.274
$TRN_1-TC_2 \times TRN_3-TC_3$	-	-0.106	-	0.669
$TRN_2-TC_2 \times TRN_2-TC_3$	-	-	-	0.345
$TRN_2-TC_2 \times TRN_3-TC_3$	-	-	-	-0.192
$TRN_2-TC_3 \times TRN_3-TC_3$	-	-0.124	-	0.399

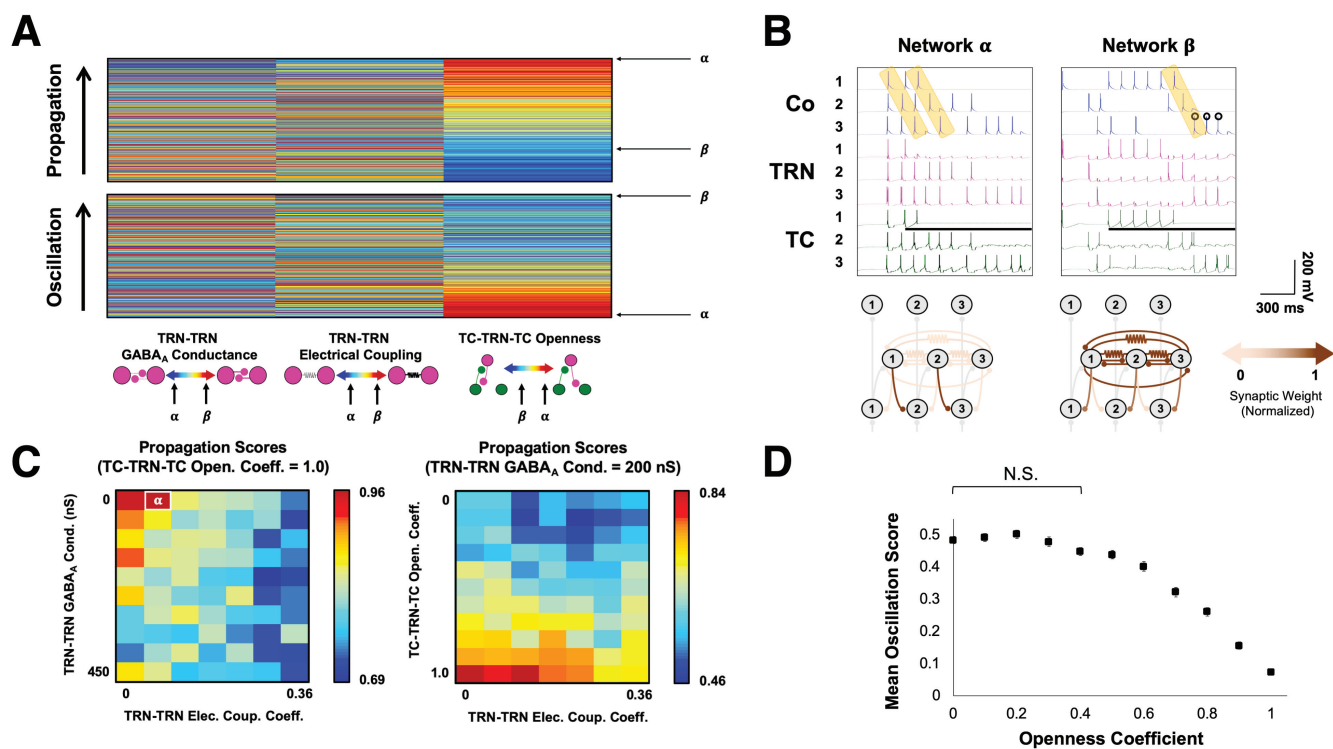
1094

1095 **Table 4.** Normalized linear and second-order regression coefficients for propagation and oscillation in  
1096 heterogeneously varied synaptic networks. The regressions include 1°, 2°, and interaction terms  
1097 corresponding to the 14 variable synapses in the networks. Equal signs denote gap junctions. Linear  
1098 regression for propagation,  $R^2=0.742$ ,  $RMSE=0.069$ ,  $p<0.0001$ ; second-order regression for propagation,  
1099  $R^2=0.857$ ,  $RMSE=0.051$ ,  $p<0.0001$ ; linear regression for oscillation,  $R^2=0.253$ ,  $RMSE=0.131$ ,  $p<0.0001$ ;  
1100 second-order regression for oscillation,  $R^2=0.388$ ,  $RMSE=0.118$ ,  $p<0.0001$ .

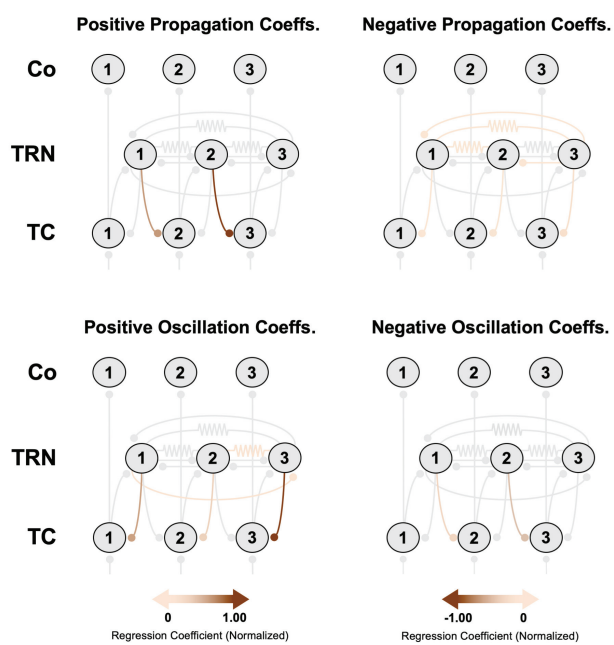
1101 **Extended Data:**

1102 **Extended Data 1.** Raw and analyzed data and simulation and analysis code generated during this study.





**A**



**B**

